STUDY OF DAMAGE IN CONCRETE BASED ON MICROSCOPIC CHANGES IN DENSITY

A Dissertation

by

PAVITRA TEJASWI MURRU

Submitted to the Office of Graduate and Professional Studies of
Texas A&M University
in partial fulfillment of the requirements for the degree of

DOCTOR OF PHILOSOPHY

Chair of Committee,	Zachary Grasley
Co-Chair of Committee,	K.R.Rajagopal
Committee Members,	Alan Freed
	Dallas Little
Head of Department,	Robin Autenrieth

December 2019

Major Subject: Civil Engineering

ABSTRACT

Damage in concrete has been modeled using various approaches such as fracture mechanics, continuum damage mechanics and failure envelope theories. The current research proposes a new approach to model damage in concrete that addresses the limitations associated with the existing approaches. The proposed density driven damage mechanics (D3-M) approach defines damage in terms of changes in the density of the material at the microscopic level where such changes are induced by mechanical and chemical loading. The suggested approach is used to simulate the response of 2D concrete bodies to uni-axial tension and uni-axial compression. The simulation results indicate that the proposed model, by means of a single constitutive function, is able to correctly predict failure patterns and aptly capture the damage mechanisms under both uni-axial tension and uni-axial compression loadings using only the information related to the microstructure, the density field and the stiffness field. D3-M model, further, is used to model chemical and chemo-mechanical damages. It is based on the premise that low-density regions are created when concrete is subjected to a chemical attack or a coupled chemical-mechanical loading resulting in reduced stiffness and strength of the material. It is also highlighted that the response of the material to a scenario where chemical and mechanical loads are acting simultaneously cannot be considered equivalent to the response obtained by superposing the responses to mechanical and chemical loads acting separately. The D3-M modeling approach stands out among the past efforts to predict the response of concrete to mechanical and chemical loading scenarios due to its ability to effectively model the mechanical, chemical as well as the coupled mechanical-chemical responses of concrete using a single constitutive equation for both types of damage.

To Amma, Nanna, Nikhila

ACKNOWLEDGMENTS

I would like to first and foremost thank Dr. Zachary Grasley, who has been the most encouraging and supportive adviser one could ask for. I have learnt from him the significance of learning by questioning and through discussion, in addition to a multitude of things related to my research.

I would like to express my sincere gratitude to my co-adviser, Dr. K.R.Rajagopal for his able and expert guidance over the course of my PhD. I am immensely thankful for all the invaluable insights I got from his many lectures and academic discussions.

I would like to express my sincere gratitude to my committee members, Dr. Alan Freed and Dr. Dallas Little for their insightful suggestions. I would like to thank Dr. Edward Garboczi for his valuable inputs.

I am thankful to Christa Torrence for providing me with the microstructure images needed for my simulations. I extend my thanks to Dr. Xijun Shi for letting me use his experimental work for my model validation. I would like to thank Dr. P.Alagappan and Dr. Zhi Yuan for helping me with my questions, related to mechanics and modeling, many times during my PhD.

It has been a great joy to have had worked amidst the best lab-mates –Manoj, TJ, Juan, Akshay, Bhaskar, Hisasi, Choi, Sai. I am glad to have met and known Sravani, Susmitha, Abhijeet, Nirup, PP, Srinath, who had been my home away from home during the past few years. I cannot thank enough 3D, Prabhas, Rini, Vigny, Swetha for being there always.

Most of all, I am grateful for my parents and my sister, without whose encouragement and support, this phase of my life wouldn't have begun and ended the way it did.

CONTRIBUTORS AND FUNDING SOURCES

Contributors

This work was supported by a dissertation committee consisting of Professor Zachary Grasley [adviser] and Professor Dallas Little of the Department of Civil Engineering, Professor K.R. Rajagopal [co-adviser] and Professor Alan Freed of the Department of Mechanical Engineering.

All other work conducted for the dissertation was completed by the student independently.

Funding Sources

Graduate study was supported by a research assistantship from Texas A&M University.

NOMENCLATURE

CDM	Continuum Damage Mechanics
LEFM	Linear Elastic Fracture Mechanics
ITZ	Interfacial Transition Zone
CH	Calcium Hydroxide
D3-M	Density Driven Damage Mechanics
RAP	Reclaimed Asphalt Pavement
FEM	Finite Element Method
BEM	Boundar Element Method
CCM	Cohesive Crack Model
FCM	Fictitious Crack Model
CBM	Crack Band Model
TPFM	Two-Parameter Fracture Model
C-S-H	Calcium Silicate Hydrate
LVDT	Linear Variable Differential Transformer
COV	Coefficient of Variation
SD	Standard Deviation
PCC	Portland Cement Concrete
STS	Splitting Tensile Strength
TxDOT	Texas Department of Transportation
ASR	Alkali-Silica Reaction
SE	Standard Error

TABLE OF CONTENTS

Page

LIST OF FIGURES

LIST OF TABLES

1. INTRODUCTION

1.1 Background and motivation

One of the key concerns related to a civil engineering structure is its life span in the sense that it is structurally integral and durable for an intended service life. In order to have a long-lasting structure, it is as important to use a durable material for its construction as it is to implement a sound structural design. In fact, by improving the quality of the material, the large safety factors that are typically used in the design process can be significantly brought down, which cut down the costs involved. Hence, a reliable manner of studying damage in a material could prove structurally and economically useful.

Since concrete is the most widely used construction material, it could be of value to have a thorough understanding of the different mechanisms involved in the damage/failure of concrete. The most common form of stimulus that affects concrete is mechanical loading. In addition, concrete is significantly affected by chemical attacks such as leaching of calcium ions, alkali-silica reaction, carbonation, sulfate attacks etc. Therefore, modeling of damage in concrete should primarily consider both mechanical effects and chemical degradation.

Traditionally, damage in concrete has been modeled mainly using two approaches: fracture mechanics and continuum damage mechanics (CDM). While fracture mechanics considers damage in a discrete format, CDM analyses smeared damage in a continuum setup. In addition, there are studies that have used failure envelope theories to define damage in concrete. Although these three approaches discuss damage/failure, they differ in their fundamental principles. While fracture mechanics is based on the assumption that the material is already cracked, continuum damage mechanics looks at the evolution of the material from undamaged to damaged. On the other hand, failure envelope theories define an "envelope curve" to predict how far a material is from failure at a particular state of stress or strain. These approaches are further discussed in the next chapter. The damage models based on the existing theories have certain limitations despite the fact that

they are often able to simulate the experimental results with reasonable accuracy. One of the specific concerns with the widely used linear elastic fracture mechanics (LEFM) based approach to model damage in concrete is that the stresses at the crack tip shoot up to infinity implying that the corresponding values of strain should be very high due to the underlying assumption of a linear stress-strain relation [2] [3]. The high strain is incompatible with the initial assumption that the displacement gradients are small based on which the theory of LEFM has been developed. To overcome this limitation, certain studies have used a non-linear constitutive function for stress in terms of strains [4]. The problem with this approach is that the strains used are based on the linearized theory of elasticity, where it is assumed that the higher order strains are negligible. This contradicts the use of most non-linear constitutive models [5]. Furthermore, the theory of fracture mechanics does not take into account the distributed potential damage due to various inhomogeneities present in concrete and instead lumps it all into a single line, which is not an accurate representation of the real microstructure of the material. In addition, the distribution of flaws and micro-cracks is likely to depend on the size and the shape of the specimen and also on the type of loading. Hence, the approach of replacing a group of micro-cracks with a single large crack for the sake of analysis might lead to major biases with respect to size (size-effect) and type of loading. Fracture mechanics also describes damage (fracture) primarily in terms of crack width, stress intensity factors and strain energy but does not address the evolution, over the course of loading, of properties such as the density, stiffness and porosity; these properties are often critical to in-service performance of a concrete structure.

Deficiencies in fracture mechanics were overcome to an extent by the researchers working on continuum damage mechanics (CDM) in concrete [6]. CDM defines damage in the form of a “damage variable" that is expressed as a function of stress or strain tensor components or their invariants [7] [8] [9] [10] [11]. But this definition has a problem at the fundamental level if looked at from the perspective of classical continuum mechanics. The stress and strain values are not absolute measures; that is, their values depend on the choice of the reference configuration, which is generally (not necessarily) chosen to be the stress-free configuration [12] [13]. For example,

let us consider the configuration at time t=0 as $\kappa 0$, the configuration at time t=t1 as $\kappa 1$ and that at time t=t2 (say t2>t1) as $\kappa 2$. Now, if we assume $\kappa 0$ to be the reference configuration and the stress-free configuration, the stress values at t2 are different when compared to a scenario where $\kappa 1$ is considered to be the reference and the stress-free configuration. This problem of ambiguity associated with the choice of reference configuration holds true with the strain values as well. Thus, by considering stress and/or strain values or any measure based on stress or strain like energy based measures as parameters to quantify damage, we are proposing that the intensity of damage is dependent on how we define our reference configuration, leading to ambiguity and subjectivity.

1.2 Scope of dissertation

Concrete is an inhomogeneous material that is composed of various flaws such as pores (gel and capillary), micro-cracks, and the interfacial transition zone (ITZ) even before it is exposed to any kind of conventional loading and these flaws are spatially distributed in a random manner. When the material is subjected to loading, these flaws enlarge and propagate, leading to the formation of larger cracks that are usually visible to the naked eye. Thus, it can be said that damage is associated with change in certain properties of the material such as density, elastic modulus, porosity etc., induced by cracking, which is initiated by already existing flaws, pores or micro-cracks.

When concrete is subjected to mechanical loading, the so-called “weak" portions (ITZ, pores and micro-cracks) in the material tend to get affected first. The “weakness" of these portions could be their low densities or high porosities. Similarly, when concrete is affected by a chemical attack such as the leaching of calcium hydroxide (CH), low density regions are created due to removal of calcium ions. As these low-density/high-porosity regions propagate with progress in mechanical/-chemical loading, the level of damage in concrete increases. Furthermore, density of a material is a real measurable parameter in an absolute sense as opposed to subjective quantities like stresses and strains that are used to define damage traditionally. The objective of this research is to develop a density driven damage mechanics (D3-M) model for concrete that has the definition of damage in terms of changes in density at a microscopic level in the material [12] [13]. Such an approach avoids the limitations of fracture mechanics and conventional CDM. The proposed damage model

aims to be able to predict the response of concrete to mechanical loads, chemical attacks and scenarios with these mechanisms acting simultaneously. The advantages of the proposed model to study damage in comparison to the existing approaches are listed in Table 1.1.

Table 1.1: Advantages of the proposed density driven damage mechanics (D3-M) model over competing approaches

Feature	Fracture Mechanics	Conventional CDM	3D-M
Simultaneous chemical & mechanical degradation	✗	✗	✓
Single constitutive equation for all stress states	✗	✗	✓
Properly handles kinematics	✗	✓	✓
Quantifies strength reductions	✓	✓	✓
Quantifies stiffness reductions	✗	✓	✓
Non subjective constitutive model	✓	✗	✓

In summary, the following tasks are defined to meet the objective of the current research, which is to develop D3-M approach for concrete that can model the response of concrete to the following scenarios:

- Purely mechanical stimuli: uni-axial tensile and uni-axial compressive loading conditions
- Mechanical degradation of concrete with reclaimed asphalt pavement (RAP) used as coarse aggregate and validating it with experimental data
- Mechanical degradation of chemically leached concrete
- A combination of mechanical and chemical stimuli: uni-axial compressive loading of concrete undergoing leaching (of CH)

Modeling is carried out using planar geometries treating concrete as an inhomogeneous material with three components: mortar (cement paste and fine aggregate), ITZ and coarse aggregate. Though ITZ is basically a part of cement paste, it is taken as a separate region for the sake of computational ease. Model validation presented in this dissertation is done using experimental data from literature.

1.3 Dissertation outline

The dissertation is composed of the following chapters: Chapter 2 discusses some of the widely used approaches to study damage in concrete. Chapter 3 describes the use of a nonlinear model (generalized neo-Hookean model) incorporated along with the theory of density-driven-damage to predict the response of concrete and the issues associated with it. In Chapter 4, the theoretical framework for an implicit theory using linearized elasticity to study damage in terms of microscopic density changes and the modeling of the response of concrete to uni-axial tensile loading and uni-axial compressive loading conditions are presented. Chapter 5 explores the application of the model to simulate damage in concrete where ordinary coarse aggregate is replaced with reclaimed asphalt pavement (RAP). In Chapter 6, the modeled response of leached concrete subjected to mechanical loading is compared with the data obtained from literature. It also presents the response of concrete subjected to mechanical loading while undergoing chemical leaching using D3-M approach. Lastly, the conclusions and the scope for future work pertaining to the current research are discussed in Chapter 7.

2. EXISTING APPROACHES TO STUDY DAMAGE IN CONCRETE

Modeling of damage in concrete has been carried out based on mainly three approaches: i) fracture mechanics, ii) CDM, and iii) failure envelope theories. Fracture mechanics is based on the assumption that a crack or a flaw is already present in the material before the application of the mechanical load. On the other hand, CDM and failure envelope theories study the progress of the material from an undamaged state to damaged state. This chapter briefly describes these three existing approaches in the following sections.

2.1 Fracture mechanics

The term "fracture mechanics" refers to a vital specialization within solid mechanics in which the presence of a crack is assumed, and it is aimed to find quantitative relations between the crack length, the material's inherent resistance to crack growth, and the stress at which the crack propagates at high speed to cause structural failure [14].

LEFM is originated by Griffith [15] who proposed the energy criterion of failure, the basis of classical LEFM, which states that "the crack will propagate if the energy available to extend the crack by a unit surface area equals the energy required to do so" [16]. Then, Irwin introduced the concept of the stress intensity factor K_I as a parameter to denote the intensity of stresses close to the crack tip and developed a relation between stress intensity factor and the energy release rate G_I [17]. Specifically, LEFM can be defined as the study of stress and displacement fields in the region of a crack tip in materials that are elastic, homogeneous, and isotropic, particularly at the onset of unstable crack growth (or fracture) [18]. The theory of LEFM is primarily based on two parameters: the critical strain energy release rate (G_{Ic}) and the critical stress intensity factor (K_{Ic}). K_I is a representation of the stress and displacement fields in the region of a crack-tip. It is considered that when this parameter attains certain critical value, usually denoted as K_{Ic}, it leads to unstable fracture. G_I is an alternative used in place of K_I at times and their critical values are

related as

$$G_{Ic} = \frac{K_{Ic}^2}{E'} \tag{2.1}$$

such that,

$$E' = \begin{cases} E & \text{For plane stress} \\ \frac{E}{1-\nu^2} & \text{For plane strain} \end{cases} \tag{2.2}$$

where E is the Young's modulus and ν is the Poisson's ratio. In this case, when G_I is used in place of K_I, it is assumed that the unstable extension of crack occurs when G_I reaches the critical value, G_{Ic} [19].

Kumar and Barai suggested that the concepts of linear elastic fracture mechanics may be reasonably characterized using a single parameter, which is the stress intensity factor [20]. The reason behind this is that based on the equations developed by Irwin from the mathematical procedures outlined by Westergaard, stress and displacement fields in the vicinity of the crack tip are controlled by the stress intensity factor [17][21]. Hence, it is assumed fair to conclude that the critical values of these parameters at the crack tip can be explained using a critical value of stress intensity factor for any mode of failure and multiple studies have been carried out using this approach to model damage in concrete [22] [23] [16] [24].

On the other hand, several studies proved that the concepts of LEFM could not be applied to concrete primarily due to its relatively large fracture process zone, which is caused by its heterogeneity and the presence of large aggregates and in large proportions [20]. Irwin, Kies et al. pointed out that the size of the yielding zone ahead of the crack tip was relatively large compared to the dimensions of the structure (specimen) and hence its effect has to be considered unlike in LEFM formulation [25]. Subsequently, non-linear fracture mechanics based models have been used to study damage in concrete. Non-linear fracture mechanics is usually based on two approaches: a) finite element method (FEM) or boundary element method (BEM), b) modified LEFM concepts. While models as cohesive crack model (CCM) [23] [26], fictitious crack model (FCM) [27] [28] [29], crack band model (CBM) [30] [31] are based on the first approach, two-parameter fracture

model (TPFM) [32], R-Curve based model (SEM) [23] belong to the second type of formulation. CCM, introduced by Barenblatt and Dugdale, is one of the simplest models that outlines the entire process of fracture. A cohesive crack is a fictitious crack that is supposed to transfer stress from one face to the other. FCM is a model where stresses are not assumed to fall to zero as soon as the crack opens but that they would gradually decrease with increasing crack width. Another approach that is widely used to model damage is to represent fracture in a smeared manner. In this method, it is assumed that infinitely many parallel cracks of infinitely small opening are continuously distributed over the finite element (of analysis). CBM is a smeared-cracking model based on continuum mechanics, which incorporates constitutive stress-strain relations along with strain-softening and the requirement of the minimum size of the localization zone.

2.2 Continuum damage mechanics

When a material is subjected to external loading (direct as mechanical or indirect chemical attacks), it undergoes changes at microscopic as well as at macroscopic levels. These might accumulate or propagate to grow bigger and eventually lead to deterioration of the material, which could be termed as "material damage". This damage of material could be a change in one or more material properties (quantitative or qualitative) such as a drop in density, strength, stiffness, durability, increase in porosity etc., which makes the study of damage an important field of research. Thus, the field of continuum damage mechanics came into being, which mainly involves studying "the evolution of distributed microscopic voids along with their effects on the mechanical behavior of damaged materials from a continuum mechanics point of view" [6]. Based on CDM concepts, it is considered that the effect of microcracks at any point can be explained with the help of appropriate mechanical variables that are termed as "damage variables". Using these, it would be relatively easier to develop an approach to assess the onset and the progress of damage in a material using continuum mechanics.

In CDM, the evolution of microcracks leads to a progressive deterioration of the material stiff-

ness, which is considered as the following in the elastic domain:

$$\sigma_{ij} = C^*_{ijkl}\epsilon_{kl} \tag{2.3}$$

where, σ_{ij} is the stress component, ϵ_{kl} is the strain component, and C^*_{ijkl} is the stiffness tensor of the damaged material that is supposed to change with the progress of damage. Pijaudier-Cabot, Borst et al. assumed that the stiffness of an isotropic material remains isotropic and modified the above relation as

$$\sigma_{ij} = (1-d)C^0_{ijkl}\epsilon_{kl} \tag{2.4}$$

where, C^0_{ijkl} is the stiffness of the undamaged material and d is damage state variable assuming a value between 0 and 1. In a similar manner, Mazars, Boerman et al. developed a CDM model for the uni-axial tensile loading [7]. It is defined as below:

$$\sigma = E_0\epsilon(1-D) \tag{2.5}$$

where,

$$D = \begin{cases} 0 & \text{if } \epsilon < \epsilon_0 \\ 1 - \frac{\epsilon_0(1-A)}{\epsilon} - \frac{A}{e^{B(\epsilon-\epsilon_0)}} & \text{if } \epsilon > \epsilon_0 \end{cases} \tag{2.6}$$

ϵ_0 is the strain corresponding to the peak point on the stress-strain curve (phenomenon idealized) for uni-axial tensile loading and A, B are material constants. Extending the above formulation to three-dimensional case, it introduced the following equations:

$$\tilde{\epsilon} = \sqrt{\sum_i < \epsilon_i >_+^2} \tag{2.7}$$

ϵ_i is the principal strain

$$< \epsilon_i >_+ = \begin{cases} \epsilon_i & \text{if } \epsilon_i \geq 0 \\ 0 & \text{if } \epsilon_i < 0 \end{cases} \tag{2.8}$$

and the damage threshold is defined by:

$$f(D) = \tilde{\epsilon} - K(D) = 0 \tag{2.9}$$

such that

$$K(0) = \epsilon_{D_0} \qquad \text{(Initial Damage Threshold)}$$

Mazars then developed an isotropic elastic damage model by using the coupling of two damage variables, D_t (tensile effects) and D_c (compressive effects), which can be summarized as [33]

$$D = \alpha_t D_t + \alpha_c D_c \tag{2.10}$$

The stress and strain equations are partitioned to accommodate both tensile and compressive effects accordingly and the expressions for α_t and α_c are derived in terms of principal strains [34]. The evolution laws in the form of expressions for D_t and D_c are proposed based on experimental results. Brekelmans, Schreurs et al. introduced a damage model based on the traditional CDM concepts that also proposed a formulation for the damage equivalent strain in the damage criterion to deal with large differences in tension and compression strength by proposing an appropriate formulation [35]. This is done by using a material constant $\eta \geq 1$, to indicate the difference in damage sensitivity between tension and compression, to define the equivalent damage strain as:

$$\epsilon_d = \begin{cases} \epsilon_a & \text{if } \epsilon_a \geq 0 \\ -\frac{\epsilon_a}{\eta} & \text{if } \epsilon_a < 0 \end{cases} \tag{2.11}$$

where ϵ_a denotes the axial strain (positive for tension, negative for compression).

2.3 Failure envelope theories

Failure envelope theories study damage by defining an "envelope curve" to predict how far a material is from failure at a particular state of stress or strain. Thus, stress or strain parameters are used to define damage in failure envelope theories similar to CDM. Several different envelope theories have been used to study damage in concrete using envelopes related to one or more stress/strain parameters such as uni-axial compressive strength, uni-axial tensile strength, bi-axial strength, maximum tensile strain, maximum principal tensile strain, Mohr-Coulomb criterion, Drucker-Prager yield criteria etc., [36] [37] [38] [39] [40].

2.4 Conclusion

Although damage models based on the theories discussed above have given results that closely represent the reality, they have certain limitations. A major concern related to LEFM is that the strains around the crack tip region tend to approach infinity, contradicting the fundamental principle of the basis of linearized elasticity, which is that the strains are very small [2] [3]. As an improvement on this, studies have been carried out by using a non-linear constitutive relation for stress and linearized strain [4]. This leads to an issue that the strains used in the current context are based on the linearized theory of elasticity, alongside an assumption that the higher order strains are negligible, thus contradicting most of the non-linear constitutive theories [5]. Another concern with regard to the theory of fracture mechanics is that it does not take into account the distributed damage due to various inhomogeneities present in concrete and instead lumps it all into a specific crack path, which is not representative of a real microstructure of the material. In addition, the distribution of flaws and micro-cracks is likely to depend on the size and the shape of the specimen and the type of loading. Therefore, when a group of micro-cracks is replaced with a single large crack, there could be biases related to size and the type of loading. On the other hand, in CDM, the "damage variable" is often expressed as a function of stress or strain tensor components or their invariants. Similarly, failure envelope theories discuss failure in terms of stress/strain parameters. But the stress and strain values are not absolute measures, that is, their values depend on the choice

of the reference configuration, which is generally chosen to be the stress-free configuration [12] [13]. Thus, by considering stress and/or strain values as parameters to quantify damage, we are proposing that the intensity of damage is dependent on how we define our reference configuration, which is not appropriate. However, parameters like temperature, density, and concentration are independent of the choice of the reference configuration and can be measured at any instant of time for a given chunk of material.

3. NONLINEAR CONSTITUTIVE THEORY AND MODELING

The behavior of concrete is conventionally modeled using a linear constitutive model due to the small magnitude macroscopic strains measured experimentally for concrete. However, it is expected that some local strains, observed at a microscopic level, are larger and it would not be prudent to automatically rule out the occurrence of large displacement gradients at a localized level when treating concrete as a material with a heterogeneous microstructure. Therefore, a non-linear constitutive model is considered first as a means to characterize the various components of concrete at the micro-scale. This chapter discusses the non-linear constitutive model and the model-predicted response for concrete to mechanical loading.

3.1 Theoretical framework

Let $\mathbf{x}$ denote the position of a particle in the current configuration and $\mathbf{X}$ denote the position in the reference configuration such that the motion of the particle is represented as

$$\mathbf{x} = \boldsymbol{\chi}(\mathbf{X}, t). \tag{3.1}$$

The displacement of the particle can be written as

$$\mathbf{u} = \mathbf{x} - \mathbf{X}. \tag{3.2}$$

The displacement gradient with respect to the reference configuration is then evaluated as

$$\frac{\partial \mathbf{u}}{\partial \mathbf{X}} = \frac{\partial \mathbf{x}}{\partial \mathbf{X}} - \mathbf{I}, \tag{3.3}$$

where $\frac{\partial \mathbf{x}}{\partial \mathbf{X}}$ is called the deformation gradient, commonly represented by $\mathbf{F}$, and $\mathbf{I}$ is the identity tensor [41]. The two Cauchy Green tensors, $\mathbf{B}$ and $\mathbf{C}$ [41], are represented as

$$\mathbf{B} = \mathbf{F}\mathbf{F}^T, \tag{3.4a}$$

$$\mathbf{C} = \mathbf{F}^T\mathbf{F}. \tag{3.4b}$$

The two common strain tensors, Green-St.Venant strain and Almansi-Hamel strain [41], are expressed respectively as

$$\mathbf{E} = \frac{1}{2}(\mathbf{C} - \mathbf{I}) = \frac{1}{2}(\frac{\partial \mathbf{u}}{\partial \mathbf{X}} + \frac{\partial \mathbf{u}}{\partial \mathbf{X}}^T + (\frac{\partial \mathbf{u}}{\partial \mathbf{X}}^T)(\frac{\partial \mathbf{u}}{\partial \mathbf{X}})) \tag{3.5a}$$

and

$$\mathbf{e} = \frac{1}{2}(\mathbf{I} - \mathbf{B}^{-1}) = \frac{1}{2}(\frac{\partial \mathbf{u}}{\partial \mathbf{x}} + \frac{\partial \mathbf{u}}{\partial \mathbf{x}}^T - (\frac{\partial \mathbf{u}}{\partial \mathbf{x}}^T)(\frac{\partial \mathbf{u}}{\partial \mathbf{x}})), \tag{3.5b}$$

where $\frac{\partial \mathbf{u}}{\partial \mathbf{x}}$ is the displacement gradient with respect to the current configuration. For a single, non-reacting, continuum, the law of conservation of mass can be expressed mathematically as

$$\rho = \frac{\rho_R}{det(\mathbf{F})}, \tag{3.6}$$

where ρ is the current density, ρ_R is the reference density, and $det(\mathbf{F})$ is the determinant of the deformation gradient $\mathbf{F}$. $det(\mathbf{F})$ is the ratio of the volume in the current configuration to the volume in the reference configuration of an infinitesimal volume element and is essentially indicative of local changes in volume. Hence, if $det(\mathbf{F})$ is greater than 1, there is an increase in the volume locally and a drop in the localized density and vice versa. The most general compressible homogeneous isotropic Cauchy elastic body is represented as

$$\mathbf{T} = \psi_1\mathbf{I} + \psi_2\mathbf{B} + \psi_3\mathbf{B}^2, \tag{3.7}$$

where **T** is the Cauchy stress tensor, and ψ_i, i=1,2,3 depend on **X**, ρ, $tr(\mathbf{B})$, $tr(\mathbf{B}^2)$ and $tr(\mathbf{B}^3)$ [42] [43] [44], and tr is the trace operator. Cauchy stress can also be written as a function of a measure of strain by substituting **e** for **B** based on Eq.(3.5b) in Eq.(3.7).

The constitutive model chosen to simulate the behavior of concrete in the current research is that of a generalization of the compressible neo-Hookean body[1], which is a special sub-case of Eq.(3.7), and is represented as

$$\mathbf{T} = \alpha(det(\mathbf{F}) - 1)\mathbf{I} + \beta dev(\bar{\mathbf{B}}), \tag{3.8}$$

where $dev(\bar{\mathbf{B}})$ is the deviatoric part of $\bar{\mathbf{B}}$ such that

$$\bar{\mathbf{B}} = \frac{\mathbf{B}}{det(\mathbf{F})^{\frac{2}{3}}}. \tag{3.9}$$

The choice of the model for the current research is based on the idea that there is a clear dependence of the stiffness of the material on local density. The model parameter α is a function of the initial bulk modulus and current density and the model parameter β is a function of initial shear modulus and current density and defined as

$$\alpha = Kf(\rho) = K\bar{f}(det(\mathbf{F})) \tag{3.10}$$

and

$$\beta = Gg(\rho) = G\bar{g}(det(\mathbf{F})). \tag{3.11}$$

Here, K is the reference bulk modulus and G is the reference shear modulus. f and g are functions of ρ and $\bar{f}$ and $\bar{g}$ are functions of the determinant of **F**. A power law constitutive relation is chosen to represent both f and g as it indicates a reduction/increase in stiffness for the corresponding reduction/increase in density from the initial density for a positive exponent n. The same function

[1]This non-linear model, when linearized by neglecting the higher-order terms and considering α to be the bulk modulus and β to be the shear modulus, will take the form of the linearized elastic Hooke's law for an isotropic body.

is considered for both $f(\rho)$ and $g(\rho)$, which is shown in Figure 3.1 and can be written as

$$f(\rho) = g(\rho) = \begin{cases} (\frac{\rho}{\rho_R})^n & \text{if } \frac{\rho}{\rho_R}\ \% > \delta \\ 0 & \text{if } \frac{\rho}{\rho_R}\ \% \leq \delta \end{cases}, \tag{3.12}$$

where the values are set for n as 10 and δ as 99.935 in tension and n as 15 and δ as 99.998 in compression. The transverse tensile strains under uni-axial compressive loading are more localized than under uni-axial tension, which means they are more sensitive to mesh resolution and hence it was challenging to capture the density drop under uni-axial compression. Therefore, a higher exponent in the power law function and a lower threshold of density drop compared to the uni-axial tension case have been chosen for uni-axial compression to be able to properly predict the progress of damage. Figure 3.1 shows that $f(\rho)$ and $g(\rho)$ are defined initially as power-law functions of the ratio of current density to initial density (shown in the figure on the right hand side of Figure 3.1), which eventually drop to zero when a threshold value for the density drop is reached. That is, the bulk modulus and the shear modulus vary as a power of the ratio of current density to initial density based on Eq.(3.10) and Eq.(3.11). From Figure 3.1, it is clear that the threshold value of percentage drop in density is different for the cases of uni-axial tension and uni-axial compression for the results presented in this research. The relation between Poisson's ratio (ν), shear modulus (G) and bulk modulus (K) for a linearly elastic, isotropic material is given as

$$\nu = \frac{3K - 2G}{2(3K + G)} \tag{3.13}$$

Assuming a Poisson's ratio of 0.2 for the entire microstructure, the relation between shear modulus and bulk modulus in the current simulation becomes

$$K = \frac{4}{3}G. \tag{3.14}$$

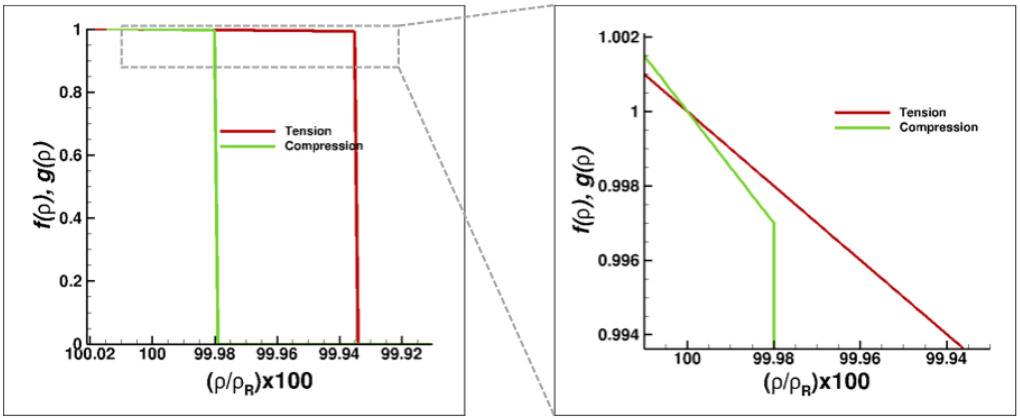

Figure 3.1: Figure showing the model parameter functions $f(\rho)$ and $g(\rho)$. Graph on the left shows the functions across the entire range of the density drop relevant for concrete in this research. Graph on the right zooms in on the initial part of the functional dependence of $f(\rho)$ and $g(\rho)$ on the density drop, which is a power law function. This initial dependence is followed by a sharp drop of $f(\rho)$ and $g(\rho)$ to zero at different values of density for tension and compression, as shown in the graph on the left.

3.2 Microstructure and modeling

The simulations are first carried out using a simplified[2] two-dimensional microstructure of dimensions 359 mm by 359 mm with three components [45]: coarse aggregates embedded in the mortar, with a thin layer of ITZ around the aggregate as shown in Figure 3.2. A two-dimensional microstructure is considered instead of a realistic three-dimensional one in order to reduce the computational costs imposed by the vastly different number of elements and run time that will be needed in 3D, considering that each ABAQUS Explicit simulation for a 2D microstructure with a mesh containing about 81000 linear elements and 55000 nodes took about 72 hours of wall-clock time on a supercomputer using 6 10-core 2.5GHz processors. The microstructure considered in this research does not have any pre-existing cracks or pores as assumed in fracture mechanics based studies. It is postulated that the failure of concrete is caused solely due to the density gradients within the three component microstructure. The details related to the generation of microstructure are discussed further in this section. Mortar is a mix of cement paste and fine aggregate (sand).

[2]The coarse aggregates are assumed to be perfectly circular unlike the irregularly shaped aggregates in reality. It is assumed that the ITZ phase around the coarse aggregates has uniform properties.

The microstructure considered has 38 % coarse aggregate by area and the thickness of the ITZ is taken to be approximately 2.6 mm, adding up to roughly 10 % by total area [46]. The modeled thickness for the ITZ is far beyond its experimentally observed range of 20 μm to 40 μm [47]. The reason for this is to avoid a large number of very small-sized elements within the ITZ zone and around the coarse aggregate-ITZ and the ITZ-mortar boundaries. Additionally, the mortar (cement paste and sand) is approximated to be a homogeneous material and hence the ITZ around sand particles is not considered as a separate component in the microstructure. These assumptions are likely to result in an under-predicted strength of the material by the current D3-M model for a given constitutive function. In turn, the fit parameters in Eq.(3.12) will be impacted by the coarsely approximated ITZ thickness. Thus, the results of the simulation provided here should not be taken to accurately represent real concrete but rather to indicate the ability of the proposed model to capture the behavior of cementitious composites.

3.2.1 About ITZ

The thin zone surrounding the aggregate particles in which the structure of the cement paste is quite different from that of the “bulk" paste farther away from the physical interface, in terms of morphology, composition, and density, is known as the ITZ or “aureole de transition" [47] [48]. It is usually 20 μm to 40 μm thick in real concrete. This region is characterized by high porosity and the reduction of unhydrated cement near the surface of the inclusion (aggregates, fibers, steel reinforcement) caused by the inability of the cement particles to pack efficiently near these inclusions (“wall effect") [49]. Within the ITZ, a gradation of porosity is usually found, relatively high at the innermost portion of this region and decreasing to the value of the bulk cement paste moving away from the aggregate surface into the bulk cement paste. Depending on the water to cement mass ratio, a maximum porosity of 50 % is observed in the ITZ region that is closest to the aggregate based on the study of Gao et al. [50]. As the density of calcium silicate hydrate, commonly referred to as C-S-H (the primary constituent of the hardened paste), is 2200 kg/m^3, the density of the ITZ can be approximated as 1100 kg/m^3 based on $\rho_{ITZ} = (1-p)\rho_{C-S-H}$, where ρ_{ITZ} is the density of the ITZ, p is the porosity of the paste and ρ_{C-S-H} is the density of

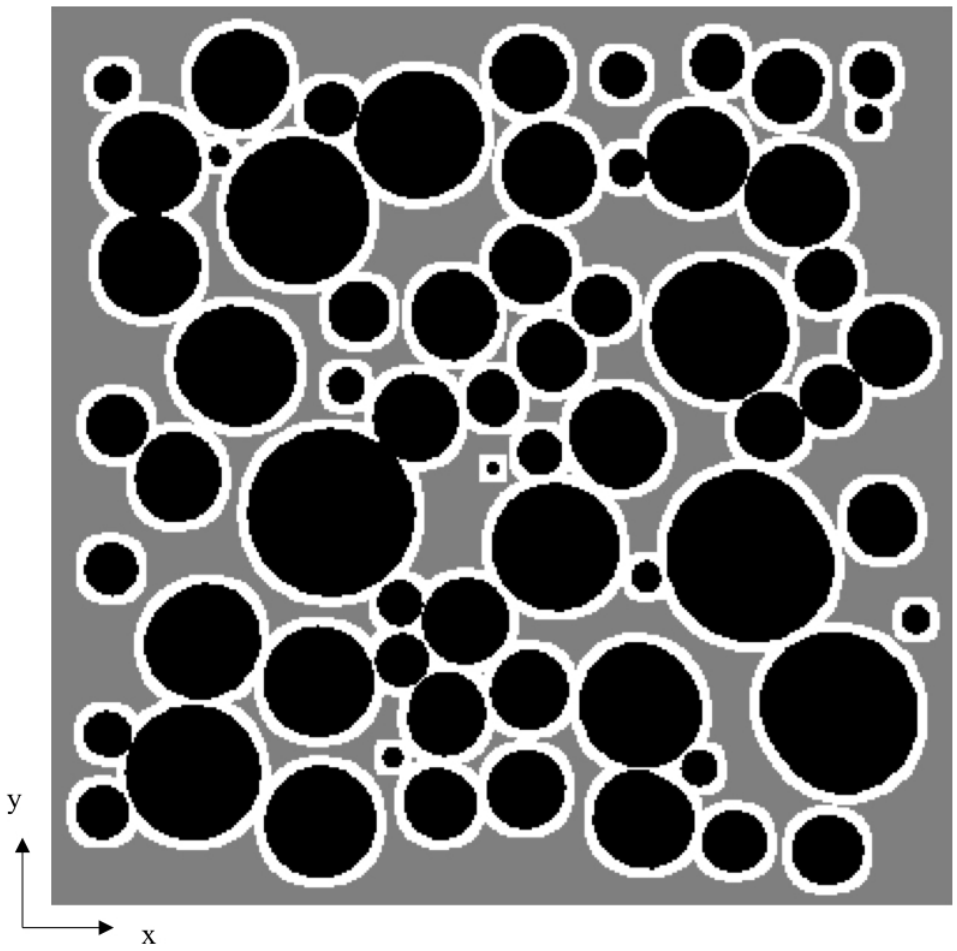

Figure 3.2: Test microstructure (359 mm by 359 mm) consisting of spherical coarse aggregates embedded in the mortar, with a thin layer of ITZ around the coarse aggregate

Table 3.1: Material properties of the three components of the microstructure

Component	Reference Density, kg/m^3	Initial Shear Modulus, GPa	Initial Bulk Modulus, GPa
Aggregate	2700	23	30
Mortar	2200	15	19.5
ITZ	1100	5	6.5

C-S-H. Here, a value of 50 % is considered for the porosity of the ITZ [50]. Based on the power law based relation proposed by W. Vichit-Vadakan et al., the elastic Young's modulus of the ITZ can be expressed as

$$E_{ITZ} = (1 - p)^3 E_{Cem}, \tag{3.15}$$

where E_{ITZ} is the elastic Young's modulus of the ITZ and E_{Cem} is the elastic Young's modulus of the cement paste [51]. The properties of the ITZ are too challenging to be measured experimentally due to its extremely small extent and the difficulty involved in distinguishing it from the actual matrix region and hence are usually empirically derived based on a model. Eq.(3.15) would lead to a elastic Young's modulus for the ITZ that is 12.5 % of the elastic Young's modulus of cement paste. But, as already mentioned, the thickness of the ITZ considered in the current research is higher than the practically observed thickness. This consideration of higher proportion of the ITZ in the microstructure is likely to under-predict the stress-bearing capacity of concrete. Therefore, the shear modulus of the ITZ is considered to be 50 % of that of the cement paste, as inferred by Hashin et al, instead of 12.5 % of the value of that of the cement paste, in order to compensate for the higher value of thickness considered in this research [52]. Based on the above discussion and Eq.(3.14), the material properties used for the three components are as shown in Table 3.1.

The microstructure is created in Wolfram Mathematica by randomly placing circles of multiple sizes ranging from 3 mm to 30 mm diameter, average size being 20 mm, in a rectangular domain to fulfill, as accurately as possible, a desired overall area fraction for coarse aggregate with a condition that boundaries of no two circles overlap with each other and no circle overlaps the sample box [53], simulating an actual piece of concrete with a mortar layer covering all the surfaces. Since

the ITZ is taken to be of constant thickness, the area percentage of ITZ in the microstructure will depend on the size of coarse aggregates for a fixed area percentage of coarse aggregates. Therefore, a large number of minimum sized aggregates will result in over-estimation of the ITZ content compared to a large number of maximum sized aggregates, thereby under-predicting the strength of the material in the former case. The image created in the previous step is first converted into an binary image and then the edges of the aggregates are detected and are further dilated to a suitable thickness to become the transition zone between the matrix and the coarse aggregates such that the area percentage of the ITZ is roughly 10 %. The resulting microstructure with three distinguishable regions is exported to OOF2, a software developed by National Institute of Standards and Technology, to mesh random 2D microstructures [54]. In OOF2, the three domains are created by manually selecting the pixels from each region and assigning a pixel group to them [55]. Then the mesh is created by choosing the element type to be a mix of quadrilateral (CPS4R in ABAQUS) and triangular (CPS3 in ABAQUS), homogeneity index of 0.99 and no horizontal or vertical periodicity. The mesh[3] is imported to ABAQUS where the material properties, load, and boundary conditions are specified. The finite element simulations are carried out in ABAQUS and not in OOF2 itself because of some in-built features available in ABAQUS such as the element deletion option and user subroutines[4] that allow the user to define certain material properties as functions of parameters related to deformation or other material properties [56]. In order to capture the post-peak strain softening (reduction of stiffness) in the response of concrete, the option of element deletion is used. This is done by defining a parameter and assigning a threshold value to it such that an element of the finite element mesh would be deleted when the parameter corresponding to that element has attained the threshold value. The parameter chosen in this research is the percentage drop in density and the threshold values are different for the cases of uni-axial tension and uni-axial compression (see Eq.(3.12) and Figure 3.1). That is, an element in the mesh is deleted if the percentage drop in density ($\frac{\rho}{\rho_R}$ %) is more than 99.935 % for uni-axial tension and it is deleted if if the percentage drop in density ($\frac{\rho}{\rho_R}$ %) is more than 99.998 % for uni-axial

[3]The mesh details are included in Appendix B

[4]The subroutine code is included in Appendix A.

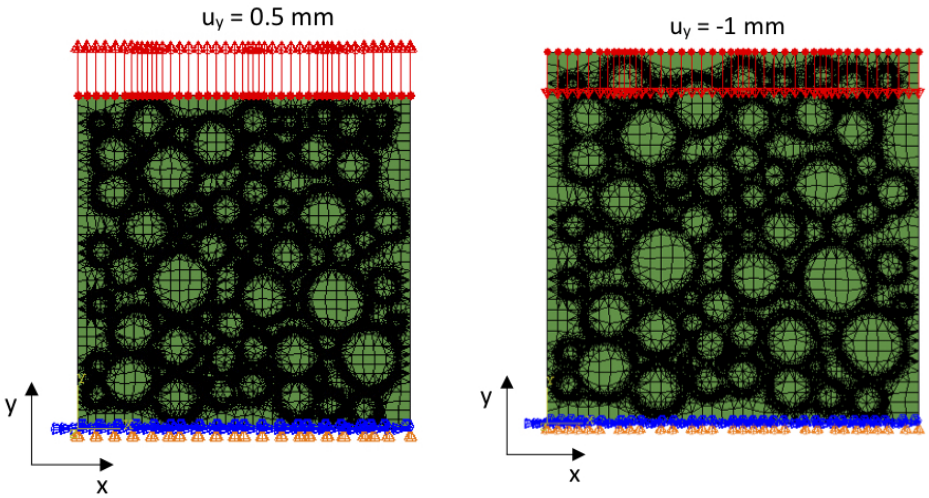

(a) A schematic representing the load and boundary conditions under uni-axial tension

(b) A schematic representing the load and boundary conditions under uni-axial compression

Figure 3.3: Schematics representing the load and boundary conditions under uni-axial tension and uni-axial compression

compression. The deleted element in the finite element simulation is essentially a damage zone in the specimen subjected to loading. Hereafter, the term “damage zone" in the context of the current research refers to the elements deleted in the microstructure due to the creation of low density regions over the course of loading.

3.3 Results and discussion

3.3.1 Uni-axial tensile loading

The test microstructure, shown in Figure 3.2, is fixed along the x-axis at the bottom edge, a displacement of 0.5 mm is applied in the y-direction at the top edge as a smooth ramp loading with amplitude increasing from 0 at time=0 to 1 mm at time=3 second in a single step while maintaining traction-free conditions along the lateral sides, as shown in Figure 3.3a. A plane stress quasi-static analysis is carried out. The density drops as the load increases due to the increased value of $det(\mathbf{F})$. This drop is relatively significant in the ITZ portion resulting in the initiation of failure in the form of damage zones in the ITZ. These damage zones propagate and/or accumulate with increased loading and lead to the failure of the specimen, which is illustrated through the drop in the axial stress-axial strain plot given in Figure 3.4. The parameter on the x-axis of this plot is the axial

strain, which is computed using the displacement of the microstructure (on the vertical edges) along the y-axis and dividing it by the gauge-length, similar to how it is done experimentally using a linear variable differential transformer (LVDT). In this case, the gauge length is the original length of the specimen along the y-axis. The axial stress parameter on the y-axis is determined by taking the average of the axial stresses undergone by all the elements along any cross-section perpendicular to the axis along which the load is applied, similar to how the stresses are computed by dividing the load applied with the cross-section area in a uni-axial loading experiment.

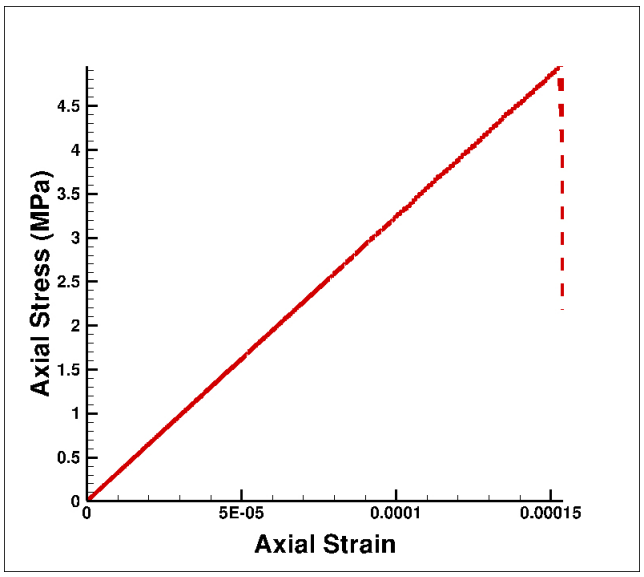

Figure 3.4: Axial stress versus axial strain plot for the uni-axial tensile loading case

3.3.2 Uni-axial compressive loading

Under the uni-axial compressive loading scenario, the microstructure is fixed along the x-axis at the bottom edge and a displacement of -1 mm is applied in the y-direction at the top edge as a smooth ramp loading with amplitude increasing from 0 at time=0 to 1 mm at time=2 seconds in a single step, as shown in Figure 3.3b. A plane stress quasi-static analysis is carried out. As the microstructure is being compressed in this case, the material tends to get denser when observed at

a macroscopic level[5]. At certain interior zones, however, there are tensile stresses developed in the lateral direction whose localized effect is expected to be greater than that due to the compressive stresses directly caused by the loading, leading to increases in volume locally. This will result in local density reductions based on the law of conservation of mass (Eq.(3.6)) in the ITZ. Thus, the failure of the material under uni-axial compressive loading is caused by the tensile stresses in the lateral direction, concentrated in the ITZ region. The propagation of damage zones and final failure is similar to that in the case of uni-axial tensile loading. The axial stress versus axial strain plot for this case is shown in Figure 3.5. The parameters on the x and y axes are computed in the same manner as in the case of uni-axial tensile loading.

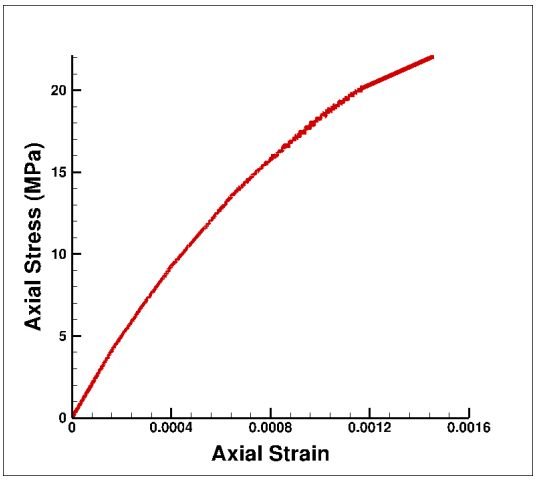

Figure 3.5: Axial stress versus axial strain plot for the uni-axial compressive loading case

The strains corresponding to peak stress for uni-axial tension and uni-axial compression are 150 microstrain and 1500 microstrain respectively, as shown in Figure 3.4 and Figure 3.5. Based on these strain values, it is determined that the small strain approximation is justified[6]. Although

[5]A linearly isotropic body with macroscopically small strains, when subjected to a uni-axial load (along y-axis), will undergo a macroscopic volumetric strain as given by $\epsilon_{vol} = (1 - 2\nu)\epsilon_{yy}$. Since $\nu \leq 0.5$, the volumetric strain (ϵ_{vol}) is negative for a negative axial strain (ϵ_{yy}). This implies that the macroscopic, homogenized density must increase for a uni-axial compressive loading.

[6]The strain value of 1600 microstrain (or 0.0016) generates a maximum error of less than 0.16%. Given the coarse microstructure approximations, this magnitude of error is deemed to be negligible.

it is hypothesized that there could be large strains at a microscopic level in concrete, it proved difficult to capture these large strains for the mesh refinement that could be achieved in the current research. A mesh sensitivity analysis done for the uni-axial compression case at three different mesh refinement levels, shown in Figure 3.6, implies that there is an increase in the maximum tensile strain captured as the mesh resolution is improved. A much finer-mesh simulation could possibly capture larger strains but could not be used owing to computational limitations as mentioned earlier. An additional possible reason for the failure to capture large local strains could be the microstructure composed of circular aggregates, which is not a very faithful representation of concrete in reality. Keeping these in mind, a linearized strain theory-based model is considered to be appropriate to study damage for concrete using the D3-M theory at the given level of mesh refinement. A microstructure with irregularly shaped aggregates positioned randomly across the domain is chosen for further analysis using a linearized strain based model. Depending on the results from this new model with the above mentioned modifications, if any large magnitude strains are observed, the non-linear constitutive model would be re-analyzed with the new microstructure.

3.4 Conclusion

Based on the results presented in the previous section of this chapter, it is clear that the strains are very small. Although it is hypothesized that there could be large strains at a microscopic level in concrete, it proved difficult to capture these large strains for the mesh refinement that could be achieved in this research. Hence, a linearized strain theory based model is considered to be more appropriate to study damage for concrete, which is discussed in the next few chapters. In addition, the microstructure used for modeling is composed of spherical aggregates (circular projections because of the planarity), which is not a very apt representation of concrete in reality. Therefore, a microstructure with irregularly shaped aggregates positioned randomly across the domain is chosen for further analysis using a linearized strain based model.

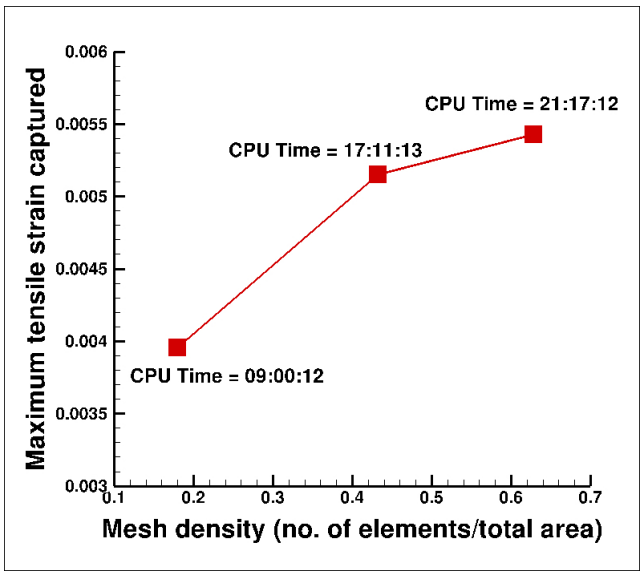

Figure 3.6: Dependence on the mesh refinement of capturing larger local tensile strains under uniaxial compressive loading using the nonlinear constitutive model. CPU Time indicates the process time for the simulation.

4. LINEARIZED STRAIN BASED DENSITY DRIVEN DAMAGE MECHANICS (D3-M) MODEL

In the previous chapter, a non-linear constitutive theory has been used to model the damage in concrete. Large strains were expected to be captured at a local level that would lead to significant drop in density leading to the damage in the material. But it was observed that the strains captured, including at local level, are very small due to limitation related to mesh resolution. Hence, a linearized strain based constitutive theory is used to model the damage in concrete. This chapter introduces the linearized strain based density driven damage mechanics (D3-M) model and presents the response of concrete to mechanical loading conditions as predicted by the model.

4.1 Constitutive model

To construct a linearized strain theory for small magnitude displacement gradients, the infinitesimal strain measure ϵ can be represented as

$$\boldsymbol{\epsilon} = \frac{1}{2}(\frac{\partial \mathbf{u}}{\partial \mathbf{X}} + \frac{\partial \mathbf{u}}{\partial \mathbf{X}}^{T}). \tag{4.1}$$

A model of the form

$$\mathbf{B} = \alpha_1 \mathbf{I} + \alpha_2 \mathbf{T} + \alpha_3 \mathbf{T}^2, \tag{4.2}$$

where α_1, α_2, α_3 depend on ρ, $tr(\mathbf{T})$, $tr(\mathbf{T}^2)$ and $tr(\mathbf{T}^3)$, when linearized will lead to

$$\boldsymbol{\epsilon} = \beta_1 \mathbf{I} + \beta_2 \mathbf{T} + \beta_3 \mathbf{T}^2 \tag{4.3}$$

such that β_1, β_2, β_3 depend on ρ, $tr(\mathbf{T})$, $tr(\mathbf{T}^2)$ and $tr(\mathbf{T}^3)$ [57]. The law of conservation of mass can be represented as

$$\rho = \frac{\rho_R}{det(\mathbf{F})} \approx \frac{\rho_R}{1 + tr(\boldsymbol{\epsilon})} \approx \rho_R[1 - tr(\boldsymbol{\epsilon})]. \tag{4.4}$$

In the current research, it is proposed that damage can be defined on the basis of changes in

density of the material, and the stiffness of the material is also affected by changes in density. Therefore, it is assumed that the evolution of the material stiffness, following from the law of conservation of mass shown in Eq.(4.4), can be represented as

$$E = E_R[1 + \gamma(\rho - \rho_R)] = E_R[1 + \gamma\rho_R[(1 - tr(\boldsymbol{\epsilon})) - 1]] = E_R[1 - \gamma\rho_R tr(\boldsymbol{\epsilon})]. \tag{4.5}$$

Here, E and E_R are the current and initial values of the Young's modulus and γ is a phenomenological coefficient. Although the value for the Young's modulus is usually determined from the values of stress and strain, in the current context, E_R is only acting as a constitutive coefficient for which we chose to assign the value of Young's modulus. The damage, here, is still being defined as a consequence of the change in the density (that is manifesting as a change in the stiffness parameter). In addition, unlike stress and strain, Young's modulus can still be measured for a chunk of material since it does not depend on any presumptions of the initial state of stress or strain when an experiment is started, but rather makes use of changes in the stress and strain from whatever the initial state may be. A value of 0.3 is chosen for γ so that the stiffness values and the values of average stress and average strain over the course of loading captured by the model are realistic for concrete. Eq.(4.5) shows that the progress of damage (evolution of stiffness) is considered to be linearly dependent on the change in density of the material. This is in coordination with the choice of a linearized strain based theory for the current research because the displacement gradients associated with the deformation are very small at the finite element mesh resolution considered herein[1]. Based on this proposition, an implicit constitutive relation for the current research is then derived from Eq.(4.3) such that $\beta_1 = -\frac{\nu}{E_R[1-\gamma\rho_R tr(\boldsymbol{\epsilon})]} tr(\mathbf{T})$, $\beta_2 = \frac{1+\nu}{E_R[1-\gamma\rho_R tr(\boldsymbol{\epsilon})]}$ and $\beta_3 = 0$ to find

$$\boldsymbol{\epsilon} = -\frac{\nu}{E_R[1 - \gamma\rho_R tr(\boldsymbol{\epsilon})]} tr(\mathbf{T})\mathbf{I} + (\frac{1+\nu}{E_R[1 - \gamma\rho_R tr(\boldsymbol{\epsilon})]})\mathbf{T}. \tag{4.6}$$

Here, E_R and ν are taken to be the initial values of Young's modulus and Poisson's ratio of the

[1]If we had chosen a Green strain or any other large strain based theory, the restriction of linear dependence of damage on density changes would not have been necessary.

material, respectively (i.e., when $\rho = \rho_R$).

The simulations are carried out using a planar microstructure of dimensions 186 mm by 387 mm with three components: coarse aggregates embedded in the mortar, with a thin layer of ITZ around the coarse aggregates as shown in Figure 4.1, the details of which would be discussed in the following section. The material properties of the three components used for the modeling are derived from the values considered for the nonlinear model shown in Table 3.1.

4.2 Microstructure and modeling

The simulated microstructure represents a section of a cylindrical core taken from a concrete structure. The simulated cylindrical core specimen (with diameter to height ratio of 1:2) is composed of randomly positioned coarse aggregates embedded in mortar with layers of the ITZ around the coarse aggregates. This is done in two steps. First, the microstructure with only the coarse aggregates and the mortar is generated using a MATLAB program [58]. The program was developed based on the Anm model developed by Qian et al. [59], and refined by Thomas et al. [60]. A mathematical description of the shape of real 3-dimensional aggregates was captured by spherical harmonic expansions, based on X-ray computed tomographic images [61]. These data are used to generate two-dimensional shapes taken from the surface projection on a third plane. The two-dimensional microstructure used for the current research is then created by grouping these shapes based on size (representing the sieve sizes typically used for concrete aggregates) ranging between 7.5 mm and 66 mm and then randomly packing these shapes into an empty domain to a required volume (area in the current context) percentage of coarse aggregates. These coarse aggregates are allowed to overlap the boundaries, with the overlapped portion cut off as happens in a real core section. This image is then converted into an binary image and the edges of the aggregates are detected and further dilated to a suitable thickness to become the transition zone between the matrix and the coarse aggregates such that the area percentage of the ITZ is roughly 10 %. A finite element mesh is finally generated in OOF2 and imported to ABAQUS as described in the previous chapter. The ITZ thickness (taken to be approximately 1.6 mm) is much larger than reality for the same reasons given previously.

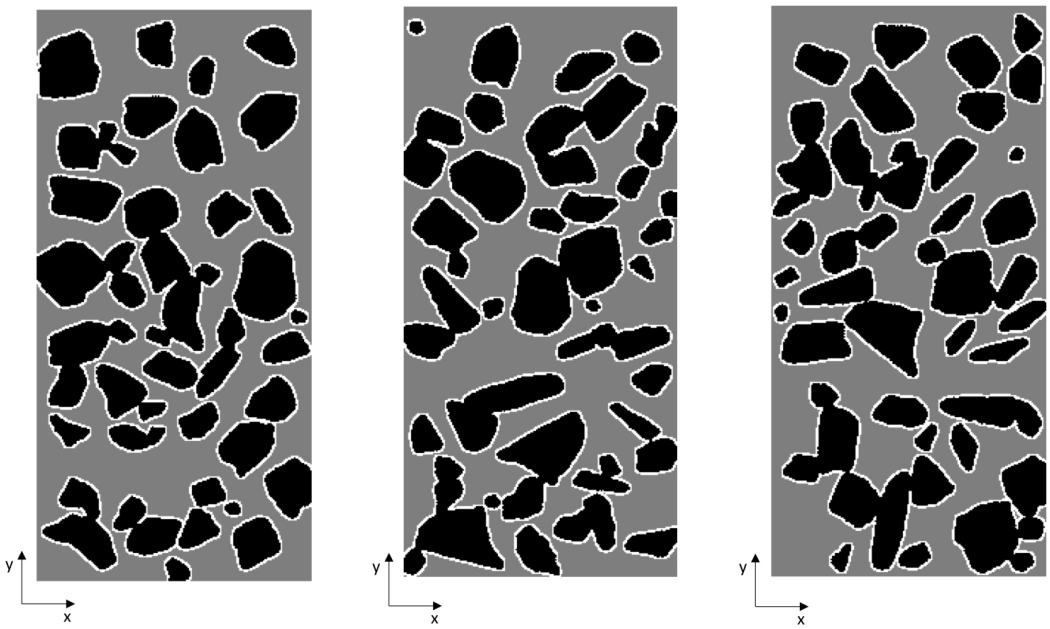

(a) Microstructure 1 (b) Microstructure 2 (c) Microstructure 3

Figure 4.1: Test microstructures (186 mm by 387 mm) representing a section of a cored cylinder using realistic aggregate shapes surrounded by ITZ

Modeling is carried out as a plane stress problem in ABAQUS in two parts: i) modeling the response of concrete subjected to a uni-axial tensile load and capturing the percentage local drop in density (corresponding value of volumetric strain) at which the material is observed to develop damage (in the form of strain softening) ii) modeling the response of concrete subjected to different loading scenarios using the volumetric strain value captured in the first simulation as a threshold value to delete damaged elements in the microstructure. ABAQUS Standard Analysis is used to carry out the first part of the modeling where a UMAT subroutine[2] is used to define the constitutive equation given by Eq.(4.6) as discussed in the previous section. An initial uni-axial tension simulation is run in order to determine the value for percentage drop in density at which there is initiation of damage in the microstructure. It is observed that the ITZ elements in the mesh begin to get damaged due to tensile stresses causing local density decay - which is inferred from the stress softening observed in these elements as shown for a single ITZ element in Figure 4.2 - at a local drop in density of 0.1 %. This is chosen to be the uniform threshold value of percentage drop in density for both uni-axial tension and uni-axial compression. Thus, unlike the nonlinear constitu-

[2]included in Appendix A

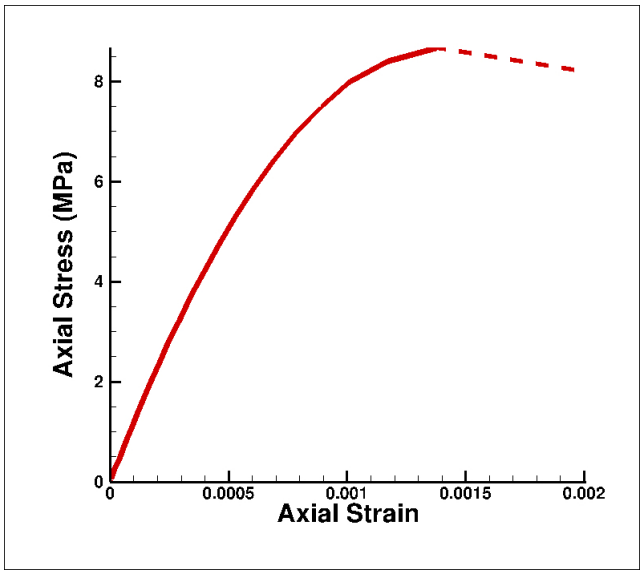

Figure 4.2: Plot showing axial stress versus axial strain for an element (of the ITZ), part of a microstructure subjected to uni-axial tension. It shows that the axial stress in the element decreases as the axial strain increases post a certain peak stress value, thus indicating local damage in the material.

tive theory, a single constitutive equation is used here to predict the damage under both uni-axial tension and uni-axial compression, in order to emphasize the theoretical premise that the damage under both these types of loadings is caused primarily by the creation of low density regions in the microstructure, which will be illustrated in detail in the following sections. The threshold value is specified as a criterion for the element deletion feature used in the next set of simulations (uni-axial tension and uni-axial compression) to delete the (damaged) elements. These simulations are carried out by using a VUMAT subroutine[2] of ABAQUS Explicit Analysis.

The simulations based on this constitutive theory used the same material properties for the three components as in case of the nonlinear constitutive model (see Table 3.1). The stiffness of cement mortar can be related to that of cement paste as presented in the experimental observations combined with theoretical results by Yang[62]. Additionally, as the stiffness of the ITZ in this research is derived from that of the cement paste, a common damage threshold for both the ITZ and the mortar is assumed. The mechanical properties of the aggregate vary from those of the mortar or the ITZ and an aggregate's damage threshold is likely to be different from that of the

other two components of the microstructure. But it is observed in the simulations of the current research that the matrix has reached failure before any of the coarse aggregates have been affected, similar to what typically happens in the case of normal strength concrete. Hence, it is deemed acceptable to have a uniform damage threshold in terms of percentage drop in density across the entire microstructure. Simulations are carried out for two types of scenarios: i) uni-axial tensile loading ii) uni-axial compressive loading. Three microstructures[3] with same proportions of each of the three components but varying in the spatial arrangement of the coarse aggregates within the rectangular domain are used for the simulations.

4.3 Results and discussion

4.3.1 Uni-axial tensile loading

The test microstructure is fixed at the bottom edge along the x-axis and a displacement of 0.5 mm is applied in the y-direction at the top edge as a smooth ramp loading with amplitude increasing from 0 at time=0 to 1 mm at time=3 seconds while maintaining traction-free conditions along the lateral sides, as shown in Figure 4.3a. A plane stress quasi-static analysis is carried out. The density drops as the load increases due to the increased value of the volumetric tensile strain. This drop is relatively larger in the ITZ portion, which results in the initiation of failure in the form of damage zones in the ITZ, as shown in Figure 4.4a. In addition, this crack path captured by the model, which is perpendicular to the loading direction is similar to the real failure plane shown in Figure 4.4b, implying that the specimen fails along the plane perpendicular to the direction of the loading in a direct tension test. These damage zones propagate and/or accumulate with increased loading and lead to the failure of the specimen, which is illustrated through the drop in the axial stress-axial strain plot given in Figure 4.5. The parameter on the x-axis of this plot is the axial strain, which is computed using the displacement of the microstructure (on the vertical edges) along the y-axis and dividing it by the gauge-length similar to how it is done experimentally using a linear variable differential transformer (LVDT). In this case, the gauge length is the original length of the specimen along the y-axis. The parameter on the y-axis is determined by taking the average of the

[3]The meshes and the mesh-details for these microstructures are included in Appendix B.

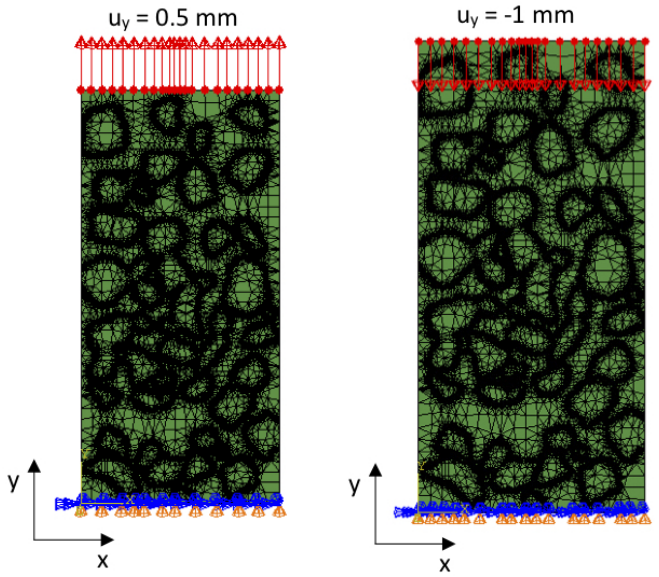

(a) A schematic representing the load and boundary conditions under uni-axial tension

(b) A schematic representing the load and boundary conditions under uni-axial compression

Figure 4.3: Schematics representing the load and boundary conditions under uni-axial tension and uni-axial compression

axial stresses undergone by all the elements along a horizontal cross-section perpendicular to the direction of loading, similar to how the stresses are computed by dividing the load applied with the cross-sectional area in a uni-axial loading experiment. Coefficient of variation (COV) for the tensile strengths predicted by the D3-M model for the three microstructures is computed as

$$COV = \frac{SD}{\mu} X 100, \tag{4.7}$$

where SD is the standard deviation and μ is the mean and its value is presented in Figure 4.5.

4.3.2 Uni-axial compressive loading

Under the uni-axial compressive loading scenario, the microstructure is fixed at the bottom edge along the x-axis and a displacement of -1 mm is applied in the y-direction at the top edge as a smooth ramp loading with amplitude increasing from 0 at time=0 to 1 mm at time=2 seconds with traction-free conditions along the lateral sides, as shown in Figure 4.3b. A plane stress quasi-

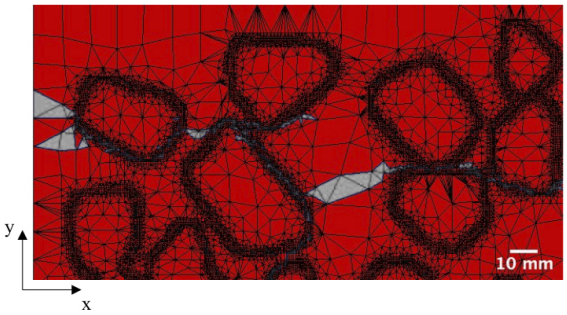

(a) Series of damage zones (shown in grey) leading to failure under uni-axial tensile loading along the y-axis (vertically)

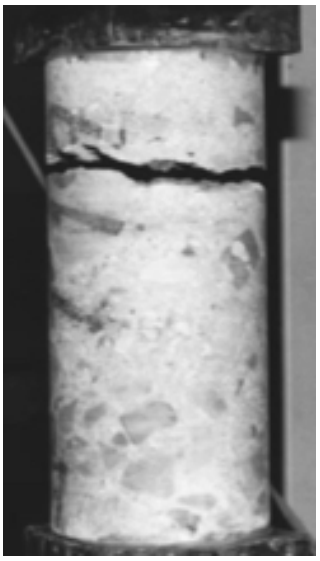

(b) Crack pattern observed experimentally under uni-axial tensile loading in the vertical direction [63]

Figure 4.4: Comparison of damage pattern under uni-axial tensile loading captured by D3-M model and observed experimentally

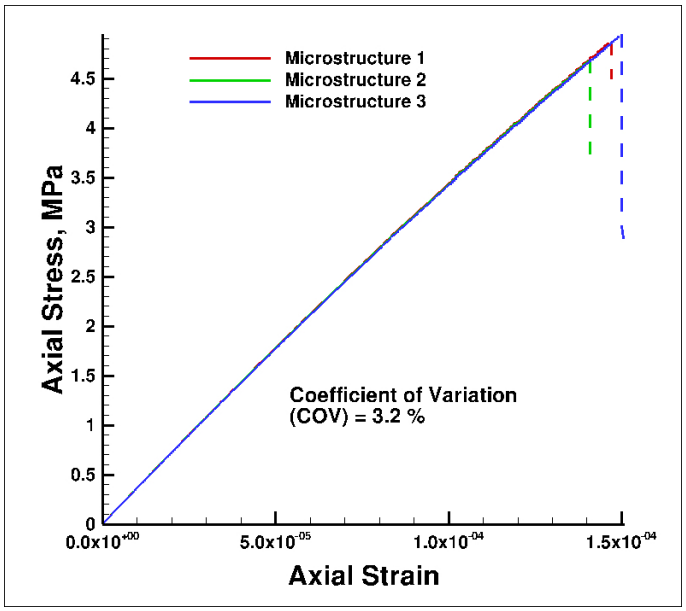

Figure 4.5: Axial stress versus axial strain plot along with coefficient of variation (COV) for tensile strengths for three concrete microstructures with 40 % coarse aggregate subjected to uni-axial tension

static analysis is carried out. As the microstructure is being compressed in this case, the material tends to get denser when observed at a macroscopic level. But there are some local areas (mainly in the ITZ regions) where the density drops just as in the tensile loading case, which establishes the fact that the failure of the material under compressive loading is also caused by the local reduction in density in the ITZ attributed to local tensile strains (stresses). Figure 4.6 shows a contour plot for the volumetric strain in a part of the microstructure. The color code for this figure is such that the regions in red have undergone the highest volumetric strain followed by shades of orange, yellow, green and finally the lowest volumetric strain regions in blue. In Figure 4.6, the red portions, which are part of the ITZ, have positive volumetric strains implying that these regions are associated with density reduction. These regions with local density decrease lead to damage zones and eventually to the failure of the specimen as shown in Figure 4.7a. This predicted damage pattern is in agreement with the crack patterns observed experimentally as shown in Figure 4.7b, where uni-axial compressive load is applied vertically (in the direction of the crack paths shown). These damage zones propagate and/or accumulate with increased loading and lead to the failure of the specimen, which is illustrated through the drop in the axial stress-axial strain plot given in Figure 4.8. The parameters on the x and y axes are computed in the same manner as explained in the case of uni-axial tensile loading. Figure 4.8 also indicates COV computed for the compressive strengths predicted by the D3-M model for the three microstructures.

COV values for the tensile and compressive strengths of the three different microstructures (with the same aggregate fractions) are found to be 3.2 % and 3.4 %, respectively, and these values are less than the COV values computed for splitting tensile strengths (6-9 %) and compressive strengths (12-21 %) measured experimentally for multiple specimens by Melis et al. [64] and Chen et al. [65]. The slightly lower predicted versus measured COV is sensible since the model captures only the variability due to the spatial distribution of aggregates, whereas experiments include additional sources of variability (e.g. cylinder end conditions and loading rates).

The results presented in this section show that the proposed D3-M theory is able to model the damage in 2D concrete models subjected to both uni-axial tension and uni-axial compression with

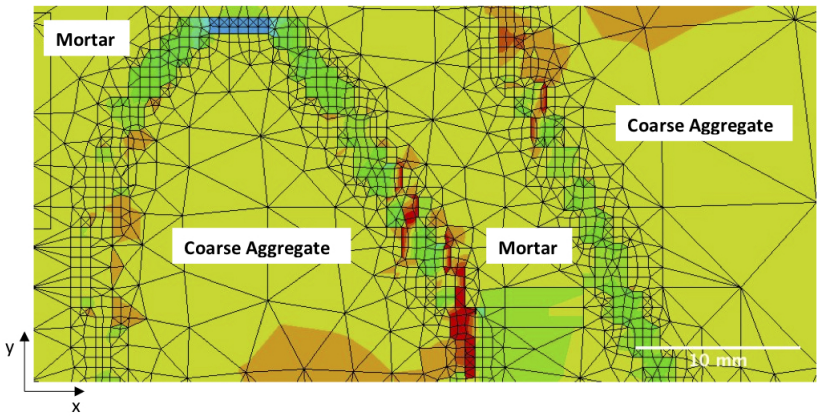

Figure 4.6: Contour plot of volumetric strain in a part of the microstructure under uni-axial compressive loading indicating positive values of the volumetric strain (bands of red) indicating local reductions in density under uni-axial compressive loading. The color code for this figure is such that the regions in red have undergone the highest volumetric strain followed by shades of orange, yellow, green and finally the lowest volumetric strain regions in blue.

the help of a single constitutive equation that is formulated based on the physical parameter of density, explaining the damage in concrete under either tension or compression. This is an improvement on the conventional CDM approach, which uses different formulations for the damage parameter (which is not necessarily physical) for tensile and compressive loading cases. Past research has recognized the need for models to capture the damage initiation and point of growth for microcracks as emanating from the ITZ [67]. However, in contrast to past approaches that force damage initiation in the ITZ, the present model is able to identify the ITZ as the weakest link in concrete naturally due to the consequence of its lower reference density in comparison to either the mortar matrix or the coarse aggregate inclusions. Indeed, predicted failure patterns in both uni-axial tension and uni-axial compression indicate realistic damage initiation and growth patterns as supported by the corresponding experimental failure patterns shown in Figure 4.4 and Figure 4.7. Damage zones propagate transversely to load in tension and parallel to load in compression.

Despite the aforementioned advantages of the D3-M approach, the model has certain limitations. The ratio of predicted compressive strength to the tensile strength for these 2D concrete models is around 21-24, which is beyond the practical range of 9-14 [47]. The drop in density due to high lateral tensile strains in the compressive loading scenario is highly localized in nature. An

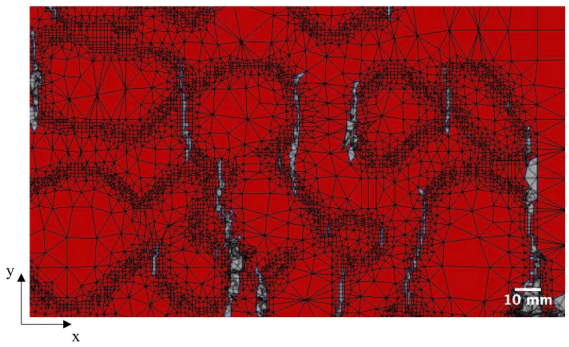

(a) Series of damage zones (shown in grey) leading to failure under uni-axial compressive loading along the y-axis (vertically)

(b) Crack pattern observed experimentally under uni-axial compressive loading in the vertical direction [66]

Figure 4.7: Comparison of damage pattern under uni-axial compressive loading captured by D3-M model and observed experimentally

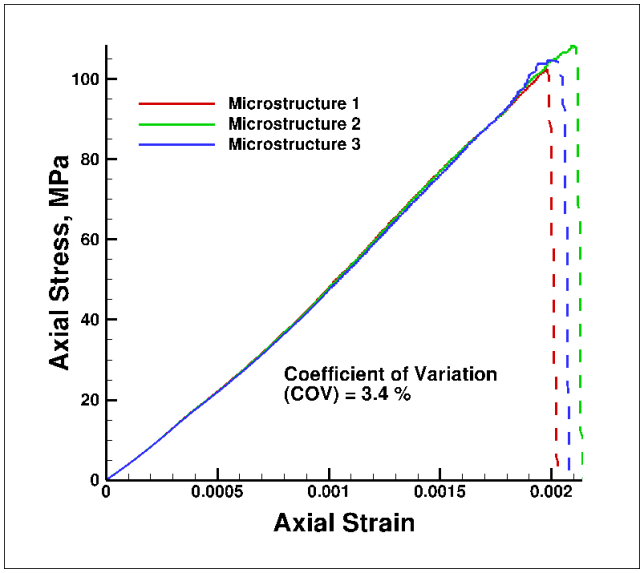

Figure 4.8: Axial stress versus axial strain plot along with coefficient of variation (COV) for compressive strengths for three concrete microstructures with 40 % coarse aggregate subjected to uni-axial compression

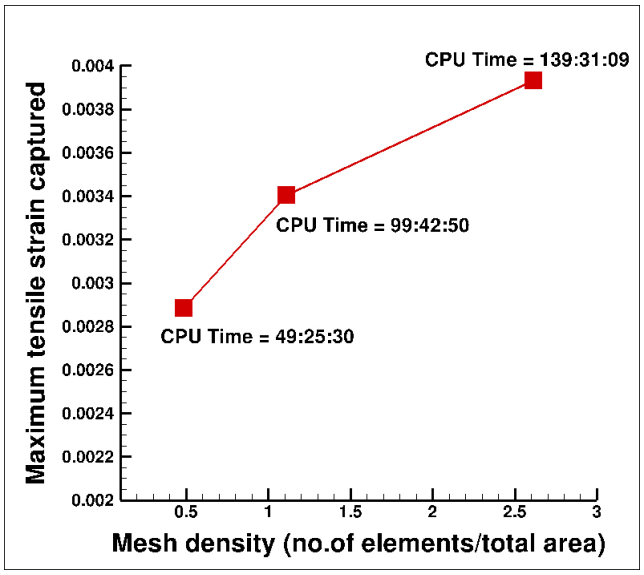

Figure 4.9: Dependence on the mesh refinement of capturing larger local tensile strains under uni-axial compressive loading using the linear constitutive model. CPU Time indicates the process time for the simulation.

increased mesh refinement is likely to effectively capture the localized tensile strains under a lower magnitude of uni-axial compressive stress as shown in Figure 4.9, but at the cost of increased computational time. Thus, if the mesh is coarser it is unlikely that the localized effects will be captured as effectively, leading to reduced element deletion and thereby an artificially increased strength in compression. In addition to these, the consideration of a 2D geometry instead of a 3D microstructure is likely to under-predict both the tensile and the compressive strengths as the 2D models lack the ability to capture the out-of-plane effects that occur in a real specimen [68] [69]. That is, coarse aggregates in a 3D microstructure are likely to pose a greater obstruction to the smooth and rapid propagation of cracks, thereby increasing the fracture resistance of concrete. It can also be observed that the strain-softening behavior observed in experiments is not captured by the model for the case of uni-axial compression. This is because of the fact that the constitutive model chosen is an elastic one and is not theoretically capable of predicting the post-peak response. It is expected that this model, when combined with an appropriate plasticity theory, could potentially predict both the elastic and softening responses to uni-axial compression in a more realistic way.

4.4 Conclusion

In the previous chapter, a non-linear constitutive model was used to simulate the damage due to mechanical loading and it was observed that the local strains were very small based on the predicted responses at the mesh resolution considered. Following this, an implicit constitutive model (D3-M model) in terms of linearized strains was developed in this chapter to simulate the response of concrete. The behavior of concrete under both uni-axial tensile and uni-axial compressive loading conditions was simulated using the same constitutive model. Using the same constitutive function for both tension and compression, the ratio of compressive strength to tensile strength was predicted to be 21-25. While these values are greater than those observed experimentally, the D3-M model is able to appropriately capture the ranking and order of magnitude difference between compressive and tensile strength using a single constitutive function. Furthermore, the D3-M model gives realistic damage patterns in both tensile and compressive loadings and is able to correctly capture the proper locations and mechanisms of damage initiation with the only a priori inputs being the microstructure geometry and the local density and stiffness fields.

5. APPLICATION OF D3-M MODEL TO PREDICT THE MECHANICAL RESPONSE OF CONCRETE WITH RECLAIMED ASPHALT PAVEMENT (RAP) AGGREGATE

5.1 Introduction

In recent times, there has been an increased demand for construction materials to accommodate the infrastructural needs of a rapidly growing society. But the affordability of natural aggregate for the growing construction works has been falling due to a combination of factors as depleted resources, increased environmental pressures and landfill tax [70]. Therefore, there has been a lot of interest currently to find out the possible ways of using recycled materials in construction materials, mainly Portland cement concrete (PCC). One such possibility is replacing, partially or completely, the aggregate in PCC with reclaimed asphalt pavement (RAP) materials. RAP aggregates are usually produced when an existing asphalt concrete pavement is repaved or rehabilitated to improve upon the deficiencies related to rutting, cracking and/or stripping. RAP materials contain both coarse and fine aggregates, with a thin layer of asphalt coated around them, which was found to be around 500 μm thick [1].

The following sections of this chapter discuss the experimental investigation carried out by Shi to determine the response of Portland cement concrete with RAP aggregate (RAP-PCC) to uniaxial compression and splitting tensile strength (STS[1]) test and further uses the D3-M model to compare the model-predicted response with the experimental results [1].

5.2 Experimental investigation

A control mix was first made using virgin coarse aggregate and fine aggregate along with a commercially available Type I/II Portland cement and class F fly ash. While the coarse aggregate was limestone with #4 (#57 in ASTM C33) gradation specified in the TxDOT standard specifications, the fine aggregate was concrete natural siliceous sand with satisfied gradation requirements by the standard specification. Additionally, a typical mid-range water reducer and an air entraining

[1]STS is an indirect measurement of concrete tensile strength.

Table 5.1: Mix Design for PCC specimens with different RAP aggregate percentages

	0 % RAP-PCC	20 % RAP-PCC	40 % RAP-PCC	100 % RAP-PCC
Cement (lb/cy)	525	525	525	525
Fly Ash (lb/cy)	131	131	131	131
Virgin Coarse Aggregate (lb/cy)	1783	1394	1021	0
RAP Aggregate (lb/cy)	0	349	681	1582
Fine Aggregate (lb/cy)	934	961	988	1071

agent were used in the mixing process. The RAP-PCC samples were made such that the virgin coarse aggregate was partially or fully replaced with a coarse RAP material. The RAP materials were provided by an asphalt concrete pavement recycler located in Bryan, Texas. The RAP replacement levels were 20 %, 40 %, and 100 % by the volume of the virgin aggregate. Mix designs for the control and the RAP-PCC mixtures are summarized in the Table 5.1.

Before mixing, all the aggregates including the virgin coarse aggregate, the RAP aggregate, and the sand were oven-dried at 105 °C for 12 hours. The moisture difference between the oven dried aggregates (assuming zero moisture) and the saturated surface dried aggregates in the mix design table was adjusted based on the absorption capacity values of the materials. Mixing was carried out with a 0.11 m^3 plastic mixer based on the standard concrete mixing practice in the lab (ASTM 192). Twelve 4 inch by 8 inch cylindrical specimens were cast for the uni-axial compression test, three specimens for each RAP percentage in the mix. The molded specimens were then placed inside a room at 23 °C for an initial curing for 24 hours, after which they were demolded and immediately transported to a standard moist curing room of 23 °C and 100 % relative humidity. The uni-axial compression test to capture the stress-strain behavior of the studied mixtures at 28 days was carried out according to ASTM C469 using an 1000-kN MTS machine. A constant displacement rate of 1 mm/min was used during the test. A ring attachment with two linear variable differential transformers (LVDTs) located at the opposite side of the attachment was utilized to record the

Figure 5.1: Experimental set-up for uni-axial compression test for RAP-PCC cylindrical specimens [1]

actual displacement of the specimen. A picture of the test is shown in Figure 5.1.

5.3 Modeling and results

Modeling in this case is carried out using the microstructure as shown in Figure 4.1a. But four different cases are considered, such that the aforementioned microstructure for each case has different percentages of RAP and virgin aggregate. This is to replicate the experimental tests described in the previous section. As already discussed, in normal strength Portland cement concrete, the cracks leading to failure usually pass through the ITZ, which has further been demonstrated in this research as shown in Figures 4.4a and 4.7a. But, it has been observed that the crack path in RAP-PCC is initiated and propagated through the asphalt layer surrounding the RAP aggregates. Therefore, the asphalt layer tends to become the critical layer around a RAP aggregate than the ITZ, in the context of damage induced by mechanical loading. This is likely to be a result of lower density and lower stiffness (Young's modulus) of asphalt than the ITZ. Hence, it is assumed, in this research, that the microstructure for RAP-PCC will be such that the transition zone between

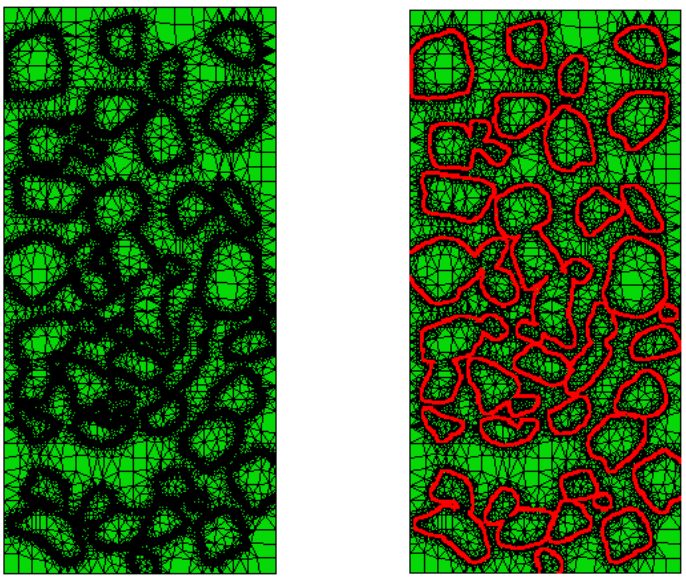

(a) Microstructure with 0 % RAP Aggregate

(b) Microstructure with 100 % RAP Aggregate

Figure 5.2: Microstructures for the two cases with single kind of coarse aggregate- either RAP aggregate or virgin aggregate. The regions with red colored boundaries are the RAP aggregates and the red colored regions are treated as asphalt mastic.

the mortar and the RAP aggregate will be asphalt and the transition between the mortar and the virgin aggregate will remain to be the ITZ. That is, it is assumed that the thickness of the asphalt layer around the RAP is assumed to be of 1.6 mm thickness, as mentioned in Chapter 4, which is higher than the experimentally observed asphalt layer thickness of around 500 μm for a RAP aggregate. This is, to an extent, compensated by not considering an ITZ layer around the RAP aggregate (between the asphalt layer and the mortar), which has been found to be more porous than the usual ITZ between the mortar and a virgin aggregate by Shi [1]. Additionally, it is possible that the model-predicted results for the cases with a mix of both RAP and virgin aggregates might be sensitive to the choice of virgin aggregates replaced with RAP aggregate in the given microstructure. Hence, three different microstructure arrangements have been considered for the two cases, where 20 % and 40 % of virgin coarse aggregate have been replaced with RAP aggregate. The microstructures for all the aforementioned possibilities are shown in Figures 5.2, 5.3 and 5.4. The summary of the composition of each of the four microstructures is as shown in Table 5.2.

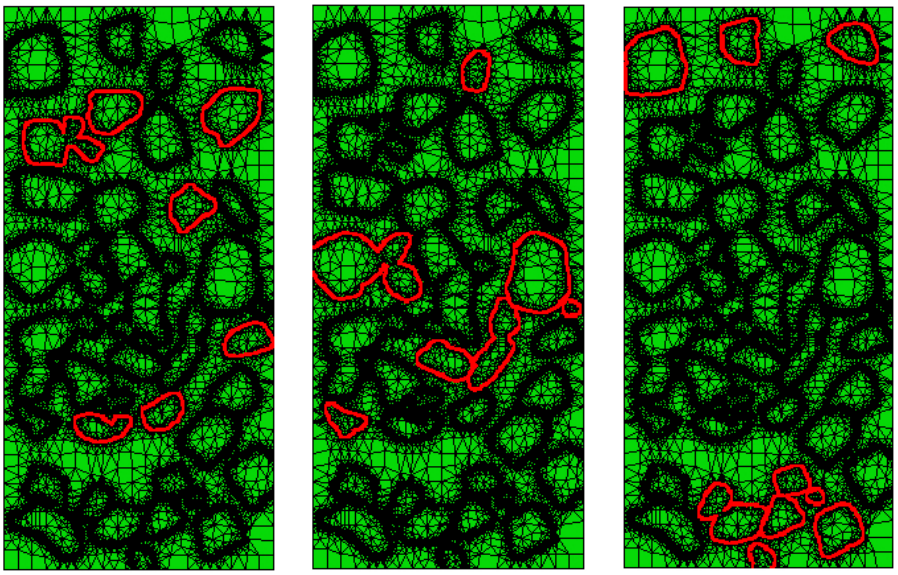

(a) Microstructure 1 with 20 % RAP Aggregate

(b) Microstructure 2 with 20 % RAP Aggregate

(c) Microstructure 3 with 20 % RAP Aggregate

Figure 5.3: Three microstructure arrangements for the case with 20 % coarse aggregate replaced with RAP aggregate. The regions with red colored boundaries are the RAP aggregates and the red colored regions are treated as asphalt mastic.

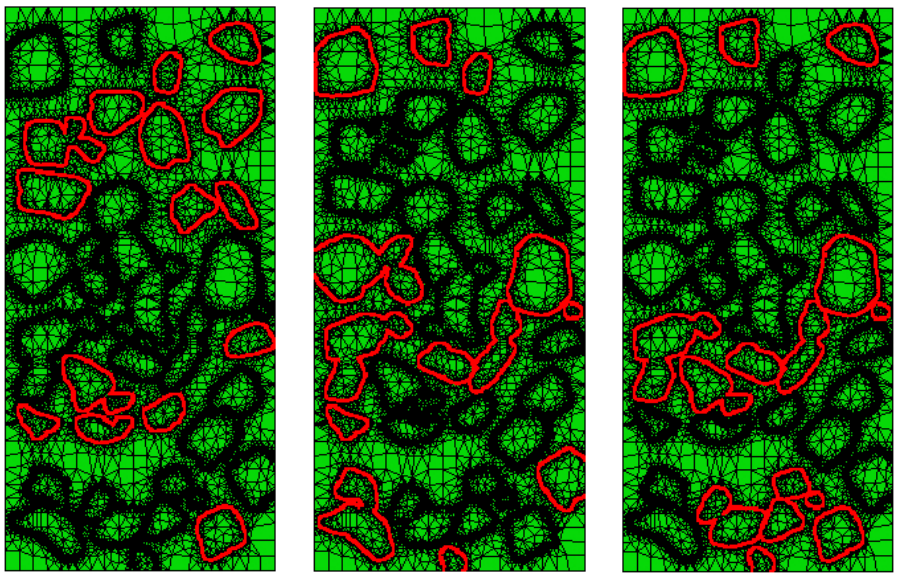

(a) Microstructure 1 with 40 % RAP Aggregate

(b) Microstructure 2 with 40 % RAP Aggregate

(c) Microstructure 3 with 40 % RAP Aggregate

Figure 5.4: Three microstructure arrangements for the case with 40 % coarse aggregate replaced with RAP aggregate. The regions with red colored boundaries are the RAP aggregates and the red colored regions are treated as asphalt mastic.

Table 5.2: Composition of the microstructure for the five different scenarios corresponding to the four experimental specimens

Microstructure	% Mortar	% Virgin Aggregate	% RAP	% ITZ	% Asphalt
0 % RAP	50	40	0	10	0
20 % RAP	50	32	8	8	2
40 % RAP	50	24	16	6	4
100 % RAP	50	0	40	0	10

Table 5.3: Material properties of the five components of the microstructure

Component	Reference Density, kg/m^3	Initial Young's Modulus, GPa	Poisson's Ratio
Coarse Aggregate	2510	55.2	0.25
Mortar	2200	34	0.2
ITZ	1100	12	0.2
Asphalt	1030	1.5	0.25

It was microscopically observed by Mukhopadhyay and Shi that the layer surrounding the aggregate in RAP is more of asphalt mastic than just the binder [71]. Additionally, the asphalt part of this layer is aged and is likely to have higher stiffness than the unaged sample. These factors make it a challenging task to assign a specific value to the stiffness to the asphalt (mastic) surrounding the aggregate in RAP. Therefore, the Young's modulus of this component is fit by trying to match the experimental data with the model prediction for the 100RAP case while assuming that the Poisson's ratio for the mastic is taken as 0.25 in one case and as 0.4 in another. The fit value for the Young's modulus, in both the cases, was 1500 MPa, which matched reasonably with the values used for modeling by Huang et al. and was within the experimentally determined range using nanoindentation by Tarefder et al. [72][73]. Hence, it was decided to consider the Poisson's ratio of the mastic as 0.25 for the rest of the simulations. It was considered that both the virgin aggregate and the RAP aggregate have same material properties and the properties of mortar and the ITZ are taken from the literature. The resulting material properties of each of the component of the microstructure are as shown in Table 5.3.

The mesh is generated in OOF2 and imported to ABAQUS for carrying out the simulation as explained earlier. The uni-axial compression test is simulated by fixing the test microstructure at the bottom edge along the x-axis and applying a displacement of -0.6 mm in the y-direction at the top edge as a smooth ramp loading with amplitude increasing from 0 at time=0 to 1 at time=2 seconds while maintaining traction-free conditions along the lateral sides. A plane stress quasi-static analysis is carried out. The stress-strain plots predicted by the model are compared with the experimental results as shown in Figure 5.5. A measure of error in the form of standard error (SE) is computed for the model-predicted result for the three sub-cases considered for each of 20 % RAP and 40 % RAP cases as

$$SE = \frac{SD}{\sqrt{N}}, \tag{5.1}$$

where SD is the standard deviation computed for three sets of model-predicted stress values corresponding to a particular strain value and N is the number of data-sets considered– 3 in the current context. Based on this measure of SE, error bars are plotted against the mean plot of the predicted result for the three sub-cases.

The results show that the D3-M model is able to predict the reduction in compressive strength values with an increase in the percentage of virgin coarse aggregate quantity that is replaced with RAP aggregate in the microstructure. The microstructure, i.e., the arrangement of coarse aggregates within the mortar, used in this research for all the four cases considered is exactly the same. The difference is that the transition zone between the mortar and certain coarse aggregates taken to be the ITZ in the microstructure of case 1 (0 % RAP aggregate) has been assigned the properties of asphalt mastic in the other three cases. That implies, the only difference between the four cases is that there are certain zones in the case 1 microstructure that are replaced by zones of lower density and lower stiffness. Therefore, the extent of these low-density and low-stiffness regions increases from 0 % RAP case to 100 % RAP case. When these microstructures are subjected to uni-axial compressive loading, there are lateral tensile strains developed locally. These tensile strains lead to density reduction locally and the already existing low-density regions have further density reductions. These zones propagate further leading to the damage of the material. Thus, greater the

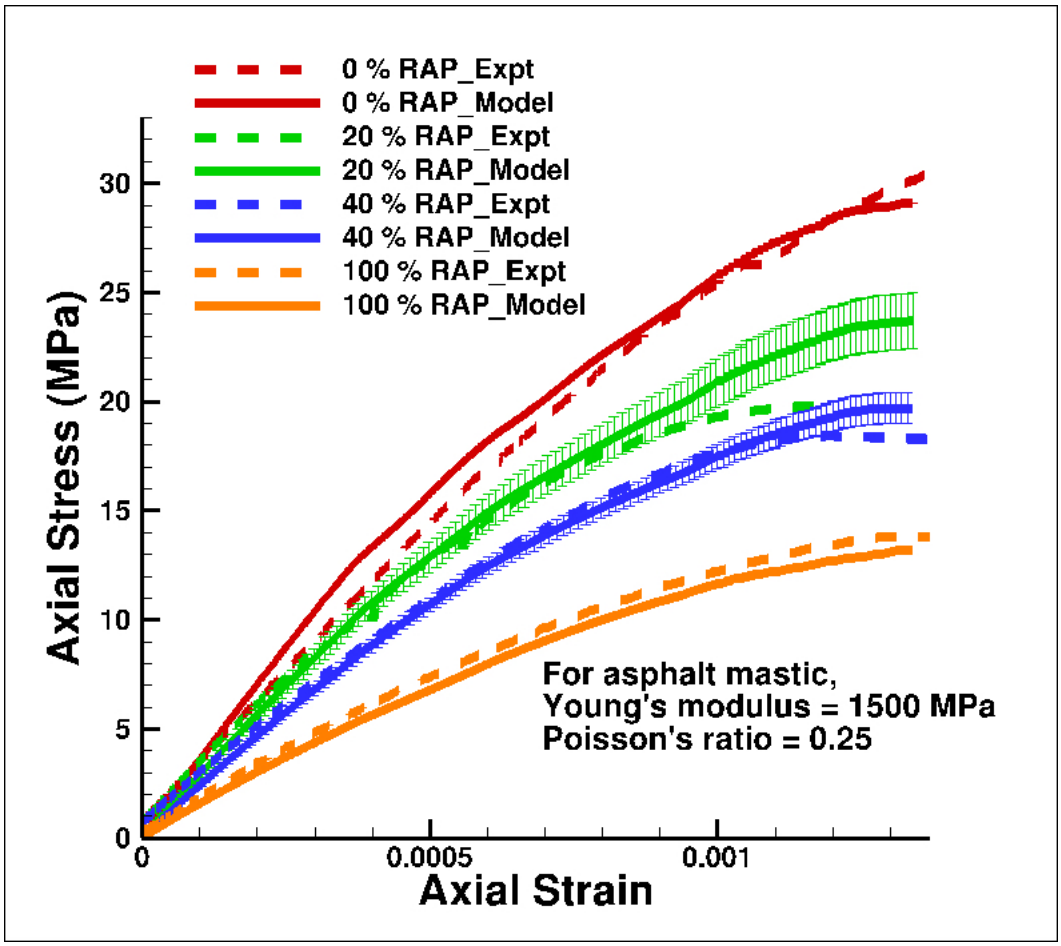

Figure 5.5: Comparison of model-predicted and experimental axial stress versus axial strain plots under uni-axial compression for four concrete microstructures with different RAP amounts. Error bars are plotted for the 20 % RAP and 40 % RAP cases using the mean plot and the standard error (SE) measure computed for three sub-cases considered based on different microstructure arrangements.

extent of the low-density regions before the mechanical loading is applied, smaller is the load that needs to be applied to cause failure.

5.4 Conclusion

The D3-M approach was applied in the context of RAP-PCC, a variant of the conventional concrete, to predict its response to uni-axial compression in this chapter. An experimental study by Shi on RAP-PCC with specimens of different RAP percentages subjected to uni-axial compression was first outlined and the experimental results were later used to support the model-predicted responses. For modeling, four different cases were considered, each with a different percentage of virgin aggregate replaced with the RAP aggregate. It was assumed that the transition zone between the RAP aggregate and the mortar is asphalt mastic as it is the ITZ between the virgin aggregate and the mortar. Since the asphalt mastic is mechanically weaker than the ITZ, the microstructure with highest RAP percentage is expected to be of the lowest strength and vice versa. The experimental trend of strength reduction with increase percentage of RAP aggregate in the microstructure could be captured by the D3-M model. Thus, the damage induced by mechanical loading as modeled by the D3-M approach could be validated with the help of experimental results.

6. MODELING OF THE RESPONSE OF CONCRETE TOWARDS CHEMICAL LEACHING

The previous chapter discussed the density driven damage mechanics (D3-M) model based on linearized strain theory. It was also demonstrated that the model could reasonably simulate the response of concrete towards uni-axial compression and uni-axial tension. This chapter presents the application of the D3-M model to predict the response of concrete to chemical leaching, emphasizing the uniqueness of the model in being able to model mechanical, chemical and coupled mechanical-chemical damages in concrete.

6.1 Existing approaches to model the response of concrete to chemical attacks and coupled mechanical-chemical loadings

Damage in concrete is caused primarily due to mechanical loads, chemical attacks and a combination of these two. Although there has been a significant amount of work done on simulating the effects of mechanical loading on the structural functionality of concrete measured through parameters such as the strength and the stiffness, the influence of chemical degradation on the same via modeling has not been sufficiently explored. There are primarily two reasons for this: i) chemical degradation almost always occurs simultaneously with mechanical deterioration of a material (in any structure) making it a very complex task to understand the effects of chemical attacks separately on the material and further model them, ii) degradation of strength and stiffness is typically modeled as a function of some measure of stress or strain magnitude, which may not prove useful in capturing chemical degradation.

In the context of concrete (cementitious materials) chemical attacks generally refer to leaching of calcium hydroxide (CH), sulfate attack, alkali-silica reaction (ASR), carbonation, chloride attack. This research is confined to modeling the effects of leaching of CH in combination with mechanical degradation for ordinary Portland cement concrete. Researchers have proposed different ways to model chemical phenomena separately and/or coupled with mechanical loads in concrete. Le Bellego et al. considered the method previously used by Gerard et al. [74] and Kuhl

et al. [75] to model chemical damage by adding a chemical damage parameter to the mechanical damage parameter in the stress-strain relation of the scalar (mechanical) damage model proposed by Mazars [34]. According to this method, damage due to chemical leaching and mechanical degradation take place entirely independent of each other such that the chemical damage parameter is solely a function of the concentration of calcium ions in the solution and the mechanical damage parameter depends on the mechanical strains [76]. Carde and Francois proposed a model to incorporate the damage caused by chemical leaching by using a damage function to describe mechanical effects and an aging function to account for chemical effects on the reduction of the elastic modulus of cement paste. While the damage function is dependent on strain, the aging function depends on calcium content in the solid phase, which in turn is defined to be a function of the depth of the degraded (leached) zone [77]. While Ulm et al. [78] modeled chemo-mechanical coupling related to leaching based on the framework proposed by Coussy [79], where the chemical damage is considered by introducing a dependence of the elastic modulus on the volume fraction of the portlandite (CH), Bangert et al. [80] modeled damage due to leaching as a scalar dependent on the local porosity in the material. Both of these preceding approaches are similar in concept to the approach proposed here since the volume fraction of a given phase is an intensive, measurable parameter that is related to local density. However, Bangert et al. and Ulm et al. apparently did not recognize that such an approach might be generalized and applied to simultaneous chemical and mechanical degradation in a unified, consistent manner.

This research aims to unify the modeling of damage associated with chemical effects and damage associated with mechanical loads using the density driven damage mechanics (D3-M) model. This includes specific tasks of modeling the mechanical damage of chemically leached concrete and modeling the damage in concrete subjected to mechanical loading while being exposed to chemical leaching. It is thereby established that the D3-M approach is appropriately able to demonstrate the effect of chemical leaching in addition to mechanical loads on the stiffness and the strength of the material.

Concrete is an inhomogeneous material that is composed of various flaws such as pores (gel

and capillary), micro-cracks and the interfacial transition zone (ITZ) even before it is exposed to any kind of conventional loading. ITZ is characterized by high porosity and the reduction of unhydrated cement near the surface of embedment (aggregates, fibers, steel reinforcement) caused by the inability of the cement particles to pack efficiently around these embedments (“wall effect"). Within the ITZ, it is usually assumed that there is a gradation of porosity, which is supposed to be relatively high at the innermost portion of this region and decreases to the value of the bulk cement paste as it moves towards the region away from the aggregate surface into the bulk cement paste. The extra pore space, originally a result of the wall effect, in concrete is mostly filled up by deposits of CH and by deposits of the calcium silica hydrate (C-S-H) passing through the solution leaving only a little extra average pore content within the ITZ [48]. Leaching of CH leads to a complete removal of the portlandite and a progressive decalcification of the C-S-H [81]. This results in replacement of the spaces filled with these materials with pores thus leading to increased porosity and hence reduced local density. Based on the D3-M theory, these low density (high porosity) regions are the source for the initiation of damage and the intensity of damage in concrete increases as these low-density/high-porosity regions propagate with progress in loading (mechanical as well as chemical). Additionally, CH is a part of the composition of both the ITZ and cement paste in concrete. Although it is inferred by Jebli et.al. that there is a significant leaching of the portlandite from the ITZ during this chemical attack based on the study carried out by Carde and François [82], it is difficult to understand in what proportions CH is being leached out of the ITZ versus the bulk paste. Hence, the possibility of CH being leached out of either or both of the ITZ and paste is explored as part of this research.

6.2 Incorporation of damage due to chemical leaching into D3-M model

Conservation of mass in conventional continuum mechanics may be expressed alternatively to Eq.(4.4) as

$$\frac{d\rho}{dt} = -\rho div[\mathbf{v}], \tag{6.1}$$

where ρ is the mass density, $\frac{d}{dt}$ is a material time derivative, **v** is the material velocity, and div is the divergence operation. From Eq.(6.1) it is clear that the only means by which a continuous chunk of material may experience density changes is from changes in volume; by definition, the material time derivative considers a fixed chunk of continuous media and direct mass losses are verboten. Thus, it is clear that conventional continuum mechanics does not provide a suitable framework for considering environmentally induced degradation that involves density changes driven by mass loss rather than strictly volume change. Mixture theory is an extension of continuum mechanics whereby one considers that, at any moment in time t, we have a mixture of N distinct species, each of which is continuous [83][84][85]. Furthermore, the mixture of these N species likewise is continuous, and occupies the same space as the mixture itself at any moment in time. At any point in the body at any moment in time, one might track the motion of any individual species with respect to itself, another species, or the mixture. Thus, one might express material time derivative of density for a given species i (within a fixed chunk of the mixture) while observing a chunk of the mixture as

$$\frac{d\rho^i}{dt} = \dot{\rho}^i_{gen} - \rho_i div[\mathbf{v}], \tag{6.2}$$

where ρ_i is the partial mass density of species i, $\dot{\rho}^i_{gen}$ is the rate of volume specific mass of species i generated within the chunk of the mixture (due to chemical reactions or phase changes of other species), and **v** is the velocity of the mixture.

The mixture of several species may be subjected to the same conservation laws as a conventional, continuous material. Thus, since the mass of the mixture is unchanging, Eq.(6.1) governs the conservation of mass of the mixture and we can define the Jacobian of the mixture as

$$J = det[\mathbf{F}] = \frac{V}{V_R} = \frac{\rho_R}{\rho}. \tag{6.3}$$

where V_R is the mixture volume in the reference configuration, ρ_R is the mixture density in the reference configuration, and ρ is the mixture density in the current configuration. Combining Eqs.

(6.1) and (6.3) yields

$$div[\mathbf{v}] = \frac{1}{J}\frac{dJ}{dt}, \tag{6.4}$$

which, when substituted into Eq.(6.2) results in

$$\frac{d\rho^i}{dt} = \dot{\rho}^i_{gen} - \frac{\rho^i}{J}\frac{dJ}{dt} \implies \frac{1}{\rho^i}\frac{d\rho^i}{dt} = \frac{1}{\rho^i}\dot{\rho}^i_{gen} - \frac{1}{J}\frac{dJ}{dt}. \tag{6.5}$$

Since the first term on the right hand side of Eq.(6.5) is associated solely with change in density due to mass of species i being generated or consumed within the mixture volume owing to chemical reactions or phase changes, we can write

$$\frac{1}{\rho^i}\dot{\rho}^i_{gen} = \frac{V}{m_i}\frac{dm^i}{Vdt} = \frac{1}{m^i}\frac{dm^i}{dt}, \tag{6.6}$$

where m_i is the current mass of species i in the mixture. Substituting Eq.(6.6) into Eq.(6.5), we get

$$\frac{1}{\rho^i}\frac{d\rho^i}{dt} = \frac{1}{m^i}\frac{dm^i}{dt} - \frac{1}{J}\frac{dJ}{dt} \tag{6.7}$$

If we integrate Eq.(6.7) from the reference configuration to some other state where deformation and/or mass changes may have occurred, we find

$$\ln\frac{\rho^i}{{\rho^i}_R} = \ln\frac{m^i}{{m^i}_R} - \ln J \implies \rho^i = {\rho^i}_R\frac{m^i}{{m^i}_R}\frac{1}{J}, \tag{6.8}$$

Eq.(6.8) describes the current, partial density of species i (ρ^i) in terms of the volume specific mass change due to production or consumption of that species, the reference configuration partial mass density of the species (${\rho^i}_R$), and the volumetric deformation of the mixture to which that species belongs, where ${m^i}_R$ is the reference mass of species i in the mixture. Thus, the first term allows one to account for changes in local density associated with chemical effects while the second term allows one to account for changes in local density associated with mechanical effects. Notice that if the mixture is comprised solely of species i, then $\rho^i \to \rho$, ${\rho^i}_R \to \rho_R$, and $m^i = {m^i}_R$, allowing

one to recover Eqs.(6.3) and (6.1) for a simple continuous body.

When the displacement gradients are small, as is usually the case with deformations in concrete, Eq.(6.8) can be written as

$$\rho^i = {\rho^i}_R \frac{m^i}{{m^i}_R} \frac{1}{(1 + tr[\boldsymbol{\epsilon}])} \approx {\rho^i}_R \frac{m^i}{{m^i}_R}(1 - tr[\boldsymbol{\epsilon}]) \tag{6.9}$$

The final constitutive equation is then derived based on the implicit equation given by Eq.(4.6) such that

$\beta_1 = -\frac{\nu^i}{E^i_R[1+\gamma(\rho^i-\rho^i_R)]} tr(\mathbf{T})$, $\beta_2 = \frac{1+\nu^i}{E^i_R[1+\gamma(\rho^i-\rho^i_R)]}$ and $\beta_3 = 0$ to find

$$\boldsymbol{\epsilon} = -\frac{\nu^i}{E^i_R[1 + \gamma(\rho^i - \rho^i_R)]} tr(\mathbf{T})\mathbf{I} + (\frac{1 + \nu^i}{E^i_R[1 + \gamma(\rho^i - \rho^i_R)]})\mathbf{T}. \tag{6.10}$$

Here, E^i_R is the initial Young's modulus and ν^i is the Poisson's ratio of the phase i of the microstructure.

6.3 Modeling and results

The microstructure used for modeling is a planar one, 186 mm by 387 mm, consisting of three components- coarse aggregates (40 % of the total microstructure area) embedded in the mortar, with a thin layer of the ITZ around coarse aggregates as shown in Figure 4.1a and is generated based on the procedure described in the earlier chapter. The simulations are further carried out in ABAQUS as plane stress problems using the constitutive equation shown in Eq.(6.10), which is formulated as a VUMAT subroutine[2] of ABAQUS Explicit Analysis.

Leaching of CH refers to removal of CH by a liquid passing through concrete. With a reduction in the volume of CH in concrete, the porosity level goes up. This leads to a drop in the density of the material. CH is a part of both the ITZ and cement paste phases of concrete. Hence, it is possible that there is density reduction in either of both of these phases when leaching happens. Two types of scenarios are simulated in this research: i) mechanical response of already-leached concrete to uni-axial compression, and ii) chemo-mechanical response of concrete that is subjected

to uni-axial compression while being leached. While the first is essentially a superposition of the chemical and mechanical responses, the latter is a coupled response. Importantly, the same model and constitutive functions are used to model both chemical and mechanical damages.

6.3.1 Leached concrete subjected to uni-axial compression

In this section, concrete specimens of different levels of degradation due to leaching are subjected to uni-axial compressive loading. That is, the mechanical response is predicted for the following cases: i) concrete that is not yet subjected to leaching, ii) concrete that is exposed to leaching for 28 days, and iii) concrete that is leached for 60 days. In the second and third cases of this scenario, concrete is first exposed to leaching alone without any mechanical loading. In this step, the value of J would be 1 (or $tr(\epsilon) = 0$) and density of each of the phase (i = ITZ, mortar) at any point during the leaching process is computed as

$$\rho^i = {\rho^i}_R \frac{m^i}{{m^i}_R} = {\rho^i}_R (1 - p^i), \tag{6.11}$$

where p^i is the porosity of the phase induced by leaching from the start of leaching process until that instant. This change in density will lead to a change in stiffness and it is assumed that the stiffness (Young's modulus) of the component will depend on the porosity based on the relation proposed by Vichit-Vadakan et al [51], which can be represented as

$$E_p^i = (1 - p^i)^3 E_s^i, \tag{6.12}$$

where E_p^i is the elastic Young's modulus of the porous phase of component i and E_s^i is the elastic Young's modulus of the solid skeleton of component i. At three levels of leaching considered in this scenario, the total porosity values would be different. The porosity values at day 0, day 28, and day 60 are observed to be 28 %, 32 %, and 36 % respectively, as determined by Huang and Qian in their study [86]. Based on these porosity values and Eqs.(6.11) and (6.12), the reference density and stiffness (Young's modulus) values are computed for the ITZ and/or mortar phases. Then the

constitutive equation defined in Eq.(6.10) is used to model the mechanical response of concrete prior to any leaching, where a value of 0.01 is found by fitting experimental data [86] for γ.

Three cases are considered for this simulation based on the possibility that CH could be leached from either or both of the ITZ and cement mortar phases. The first assumes that CH is leached from both the phases proportional to their percentage composition in the microstructure (mortar- 50 %, ITZ- 10 %). That is, an increase in total porosity by 4 % from day 0 to day 28 would mean a sixth of porosity increase in the ITZ and five-sixths increase in the mortar region. The same would be extended for leaching at 60 days. This would lead to the reference density and Young's modulus values for the ITZ and mortar at three stages of leaching as shown in Table 6.1 while the properties of the coarse aggregate would remain the same. In the second case, it is assumed that CH is leached from only the paste phase. That is, an increase in total porosity by 4 % from day 0 to day 28 would mean an increase in porosity in the mortar region by 8 % (mortar occupies 50 % of the microstructure area). The same would be extended for leaching at 60 days. This would lead to the reference density and Young's modulus values for the mortar at three stages of leaching as shown in Table 6.2 while the properties of the ITZ and coarse aggregate would remain the same as in the reference configuration. In the third case, CH is assumed to be leached from only the ITZ. This means that an increase in total porosity by 4 % from day 0 to day 28 would be equivalent to an increase in porosity in the ITZ region by 40 % (ITZ occupies 10 % of the microstructure area). The same would be extended for leaching at 60 days. This would lead to the reference density and Young's modulus values for the ITZ at three stages of leaching as shown in Table 6.3 while the properties of mortar and coarse aggregate would remain the same. Under all scenarios, constant Poisson's ratio values of 0.25 for coarse aggregate and 0.2 for the ITZ and mortar are assumed.

The microstructures with different sets of material properties, for the three cases as discussed above, are then subjected to uni-axial compression. For this, the microstructure is fixed at the bottom edge along the x-axis and a displacement of -0.7 mm is applied in the y-direction at the top edge as a smooth ramp loading with amplitude increasing from 0 to 1 with traction-free conditions along the lateral sides. A plane stress quasi-static analysis is carried out. The model predicted

Table 6.1: Material properties at three stages of leaching when it is assumed that CH is leached out of both the ITZ and cement paste

Component	No Leaching		28-day Leaching		60-day Leaching	
	Reference Density, kg/m^3	Young's Modulus (E_R), GPa	Reference Density, kg/m^3	Young's Modulus (E_R), GPa	Reference Density, kg/m^3	Young's Modulus (E_R), GPa
Mortar	2200	36	2053.3	29.3	1906.7	23.4
ITZ	1100	12	1026.7	9.7	953.3	7.8
Aggregate	2700	55.2	2700	55.2	2700	55.2

Table 6.2: Material properties at three stages of leaching when it is assumed that CH is leached out of only cement paste phase

Component	No Leaching		28-day Leaching		60-day Leaching	
	Reference Density, kg/m^3	Young's Modulus (E_R), GPa	Reference Density, kg/m^3	Young's Modulus (E_R), GPa	Reference Density, kg/m^3	Young's Modulus (E_R), GPa
Mortar	2200	36	2024	28	1848	21.3
ITZ	1100	12	1100	12	1100	12
Aggregate	2700	55.2	2700	55.2	2700	55.2

Table 6.3: Material properties at three stages of leaching when it is assumed that CH is leached out of only ITZ phase

Component	No Leaching		28-day Leaching		60-day Leaching	
	Reference Density, kg/m^3	Young's Modulus (E_R), GPa	Reference Density, kg/m^3	Young's Modulus (E_R), GPa	Reference Density, kg/m^3	Young's Modulus (E_R), GPa
Mortar	2200	36	2200	36	2200	36
ITZ	1100	12	660	2.6	220	0.1
Aggregate	2700	55.2	2700	55.2	2700	55.2

stress-strain responses are compared with the experimental observations captured by Huang and Qian as shown in Fig.6.1a, Fig.6.1b and Fig.6.1c [86].

6.3.2 Concrete subjected to leaching and uni-axial compression loading simultaneously

In this section, the response of concrete subjected to uni-axial compressive loading as it is being leached is predicted. In a scenario where concrete is subjected to mechanical load as it is exposed to leaching, density (porosity) changes simultaneously due to two factors: i) mass reduction- leaching of calcium hydroxide from the matrix leading to creation of empty spaces (pores) ii) volume increase- volumteric strains caused by tensile stresses developed locally due to mechanical loading. That is, when chemical leaching and mechanical load act simultaneously on the material, the density of each phase (i = ITZ, mortar) at any instant during the loading is evaluated as

$$\rho^i \approx {\rho^i}_R \frac{m^i}{{m^i}_R}(1 - tr[\boldsymbol{\epsilon}]) = {\rho^i}_R(1 - p^i)(1 - tr[\boldsymbol{\epsilon}]), \tag{6.13}$$

where a linear function is assumed to define evolution of porosity over time using the porosity values determined by Huang and Qian [86]—28 % at day 0, 32 % at day 28, and 36 % at day 60 respectively. Then, the above defined expression of density is substituted in the constitutive equation given by Eq.(6.10), which is used to model the response of concrete to the coupled loading. In this case, a value of 0.001 is used for γ.

Three cases are considered for this simulation, again based on the possibility that CH could be leached from either or both of the ITZ and cement mortar phases. The first one assumes that CH is leached from both the phases proportional to their percentage composition in the microstructure (mortar- 50 %, ITZ- 10 %). The second one is based on the assumption that CH is leached only from cement paste, and the third case assumes that leaching is restricted to the ITZ. The reference values of density and Young's modulus are as shown in Table 6.4.

The microstructures in all three cases as discussed above, are then subjected to uni-axial compression, with and without chemical degradation occurring simultaneously. For this, the microstructure is fixed at the bottom edge along the x-axis and a displacement of -0.7 mm is applied

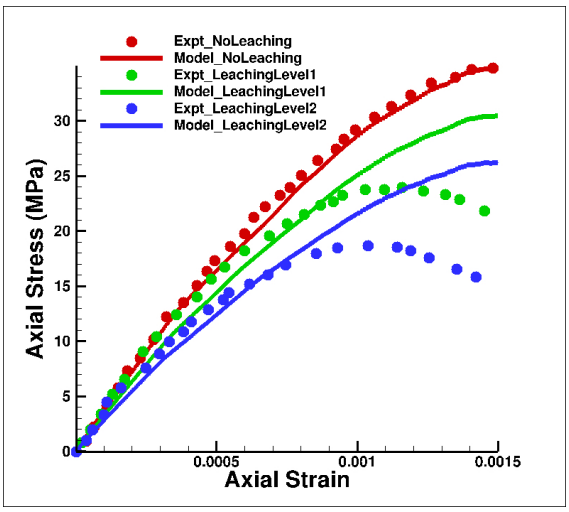

(a) Results based on the assumption that CH has been leached from both cement paste and the ITZ

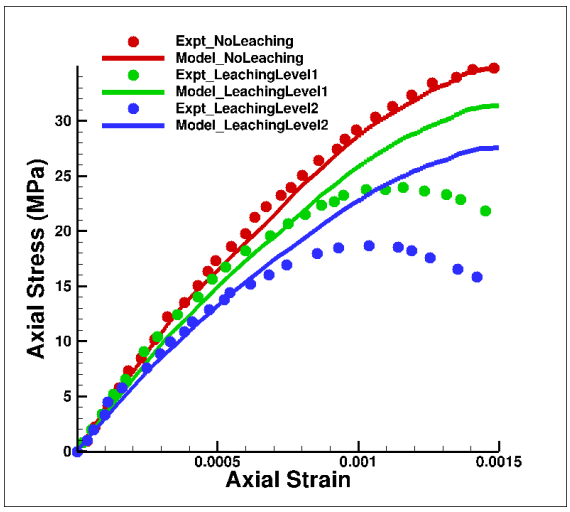

(b) Results based on the assumption that CH has been leached solely from cement paste in the specimen

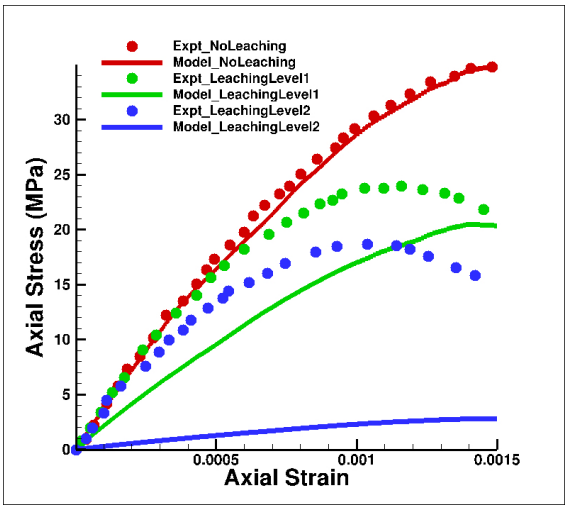

(c) Results based on the assumption that CH has been leached solely from the ITZ in the specimen

Figure 6.1: Comparison of plots showing axial stress versus axial strain for concrete microstructure (with 40 % coarse aggregate) at different levels of degradation caused by CH leaching subjected to uni-axial compression. Model was fitted to unleached data and then used to predict the leached data with three different sets of assumptions.

Table 6.4: Material properties of the three components for the coupled loading scenario

Component	Reference Density, kg/m^3	Young's Modulus (E_R), GPa	Poisson's Ratio (ν)
Mortar	2200	36	0.2
ITZ	1100	12	0.2
Aggregate	2700	55.2	0.25

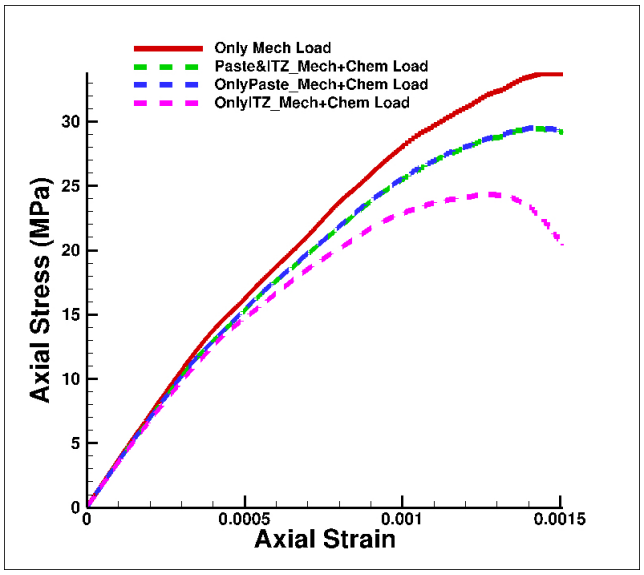

Figure 6.2: Comparison of concrete's responses to scenario of coupled leaching and uni-axial compressive loading and to that of uni-axial compression. Three cases are further considered under coupled scenario- CH leaching from both paste and the ITZ, CH leaching only from paste and CH leaching from only the ITZ. Coupled leaching and uni-axial compressive loading implies that concrete is subjected to leaching and uni-axial compression simultaneously for the entire loading period.

in the y-direction at the top edge as a smooth ramp loading with amplitude increasing from 0 to 1 with traction-free conditions along the lateral sides. A plane stress quasi-static analysis is carried out. The response of concrete in these three cases is compared with a scenario where the material is subjected to the same uni-axial compressive load but without any exposure to leaching. The comparison is shown in Figure 6.2. Additionally, the response to the coupled chemical-mechanical loading, in all three cases, is compared to the response of the material to a scenario of superposed chemical-mechanical loading (leaching is followed by uni-axial compression without any overlapping of the two loadings) as shown in Figure 6.2.

6.3.3 Discussion

The results of the scenario where concrete is first exposed to chemical leaching and then subjected to uni-axial compression show that the mechanical strength of concrete is affected due to the degradation caused by chemical leaching in the form of density reduction. Further, there is

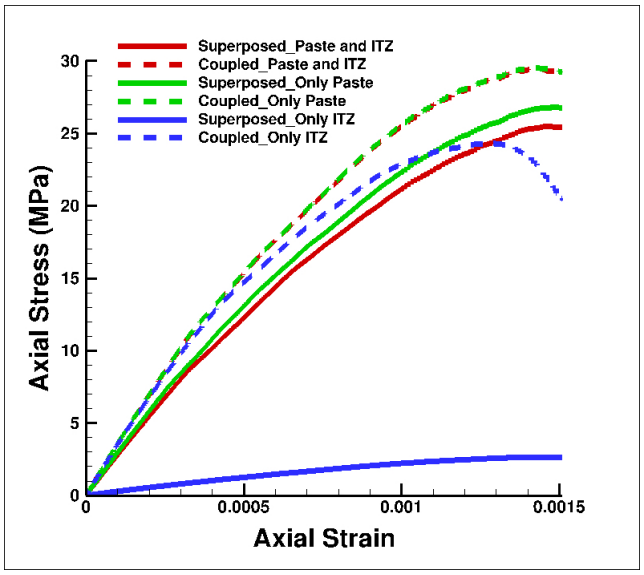

Figure 6.3: Comparison of concrete's responses to scenario of coupled leaching and uni-axial compressive loading and to that of superposed leaching and uni-axial compression. Three cases are further considered under coupled scenario- CH leaching from both paste and the ITZ, CH leaching only from paste and CH leaching from only the ITZ. Superposed leaching and uni-axial compression implies that concrete is first exposed to leaching and then subjected to uni-axial compression.

a reduction in stiffness of the material due to the mechanical loading, which is evident from the reduction in the slope of axial stress versus axial strain plots shown in Figure 6.1. When concrete is subjected to uni-axial compression, the material tends to get denser when observed at a macroscopic level. But there are some local areas (mainly in the ITZ regions) where the density drops due to local tensile strains (stresses) in the lateral direction (direction perpendicular to that of loading). As mentioned earlier, CH could be removed from either or both of the ITZ and cement paste and it is almost impossible to determine what amounts of CH are removed from each of these phases. Based on the results obtained, it is clear that the strengths are over-predicted when it is assumed that the CH is removed entirely from paste or that it is removed in quantities proportional to their volume (area) fraction in the specimen (microstructure). On the other hand, the strengths are under-predicted when it is assumed that CH is leached out solely from the ITZ. Therefore, it is most likely that CH is removed from both the ITZ and paste, the larger contribution being from the ITZ phase.

In case of the coupled chemical and mechanical loading scenario, concrete is subjected to uni-axial compression as it is being chemically leached. It would be expected that the material degradation in this case is greater than in the case where concrete is subjected to pure uni-axial compression as there would be density reduction due to both leaching and volumetric expansion caused by mechanical loading. This is supported by the model-predicted results shown in Figure 6.2. The response cannot be analyzed as a superposition of chemical and mechanical responses as this scenario cannot be treated equivalent to the case where the two stimuli act one after the other with no overlap. This is evident from the comparison of the model-predicted results shown in Figure 6.3. Thus, when modeling concurrent chemical and mechanical degradation of concrete- as is often happening in real structures- it is necessary to use a fully coupled, fully consistent modeling framework as was presented here.

6.4 Conclusion

Modeling of damage in concrete due to chemical attacks or due to a combination of chemical and mechanical loads has been a challenging task. Researchers in the past have tried to use models where the chemical damage parameter is defined using parameters such as calcium ion concentration, depth of the degraded zone etc., and the mechanical damage is defined as a function of subjective quantities like stresses and strains. In some cases, the two damages are looked at as independently acting phenomena and the others have tried to superpose the two damage parameters defined separately using mechanical and chemical attributes. In order to attribute physical significance to the models used to predict the chemical and coupled chemo-mechanical damages, the choice of a real, measurable parameter as density to quantify damage is considered apt. Hence, an implicit constitutive model (D3-M model), which defines damage in terms of density changes, was chosen to simulate the chemical and chemo-mechanical responses of concrete. The behavior of concrete was simulated using this model to predict the response under two scenarios- one where leached concrete is subjected to uni-axial compression and the other where concrete is subjected to uni-axial compression as it is being leached of CH. The model was able to predict the experimentally observed trend in reduction of stiffness and strength of concrete when it is subjected

to uni-axial compression at different levels of chemical degradation. Although the trends could be predicted, the exact strength loss in terms of magnitude could not be matched because of the uncertainty in the distribution of porosity induced by leaching across the phases of mortar and the ITZ. Unlike most of the existing approaches to model chemical damage in concrete, D3-M model is able to clearly distinguish between the scenarios of superposition of chemical and mechanical responses and of coupling of chemical and mechanical responses.

7. CONCLUSIONS AND FUTURE RESEARCH

7.1 Summary and conclusions

The study of mechanical damage in concrete has traditionally been done based on the principles of fracture mechanics,especially linear elastic fracture mechanics (LEFM), continuum damage mechanics (CDM), and failure envelope theories. Damage, in LEFM, is studied in terms of crack propagation defined on the basis of parameters like strain energy, stress intensity factor, crack width etc. It does not quantify the evolution of parameters physically suggestive of damage such as stiffness. In CDM and failure envelope theories, damage is defined in terms of quantities related to stress and strain, which are relative parameters that depend on the choice of the reference configuration. Modeling of chemical damage or coupled mechanical-chemical damage in concrete has been done in the past in different manners. Some have defined chemical damage in terms of parameters like calcium ion concentration, depth of the degraded zone etc., and mechanical damage as a function of subjective quantities like stresses and strains. In some cases, the two damages are treated as independent phenomena and the others have tried to superpose the two damage parameters defined separately using mechanical and chemical attributes. Keeping in mind some of the limitations of the existing approaches, as part of the current research, density driven damage mechanics (D3-M) model was developed in which damage is quantified in terms of density, a real measurable quantity that does not depend on the choice of the reference configuration. In addition, the choice of density to define damage enables the prediction of the response of the material (concrete in this research) without the need of any information about the stress history of the material. The choice of a quantity like density makes it simpler to associate the models predicting the chemical and coupled mechanical-chemical damages with a physical significance.

A non-linear constitutive theory based on a generalized neo-Hookean model was initially proposed where the dependence of damage on density is brought in using the law of conservation of mass. This model was used to simulate the damage due to mechanical loading and it was observed

that the local strains were very small based on the predicted responses at the mesh resolution considered. Then, an implicit constitutive model in terms of linearized strains was developed. The behavior of concrete under both uni-axial tensile and uni-axial compressive loading conditions was simulated using the same constitutive model. The same constitutive function was used to model the behavior under both tension and compression and the ratio of compressive strength to tensile strength was predicted to be 21-25. Though these values are greater than those observed experimentally, the D3-M model is able to appropriately capture the ranking and order of magnitude difference between compressive and tensile strength using a single constitutive function. The D3-M model predicts realistic damage patterns in both tensile and compressive loadings and correctly captures the proper locations and mechanisms of damage initiation with the only a priori inputs being the microstructure geometry and the local density and stiffness fields. The mechanical response predicted by the model was also validated with the help of experimental data collected for Portland cement concrete with reclaimed asphalt pavement (RAP) aggregate (RAP-PCC) subjected to uni-axial compression.

The research was also extended to model the behavior of concrete under two scenarios- one where leached concrete is subjected to uni-axial compression and the other where concrete is subjected to uni-axial compression as it is being leached of CH. The model wa able to predict the experimentally observed trend in reduction of stiffness and strength of concrete when it is subjected to uni-axial compression at different levels of chemical degradation. But the exact strength loss in terms of magnitude could not be matched because of the uncertainty in the distribution of porosity induced by leaching across the phases of mortar and the ITZ. D3-M model is also able to clearly distinguish between the scenarios of superposition of chemical and mechanical responses and of coupling of chemical and mechanical responses.

7.2 Scope for future work

The D3-M approach presents scope for certain extensions in future. The two major components of the concrete microstructure, the coarse aggregate and the mortar, have different thermal properties. Therefore, when they are subjected to thermal loads, there will be density gradient created

due to generation of non-uniform volumetric strains within the microstructure. D3-M model could be used to predict the response of concrete to such thermal loads and further to model coupled thermo-mechanical damage. The microstructure considered in the current research is composed of coarse aggregate and mortar with an interfacial transition zone (ITZ) between the two components. The D3-M approach could be extended to model damage in other materials like mortar and fiber-reinforced concrete. While mortar can be treated as an agglomeration of fine aggregates embedded in cement paste matrix with an ITZ separating the two components, fiber-reinforced concrete can be modeled by incorporating an additional component in the form of fibers into the microstructure used in the current research. D3-M model is currently able to predict the response of concrete subjected to purely elastic deformations. In future, it is intended to incorporate into the model, a capability to predict response of concrete to permanent deformations, which lead to dissipation of energy.

REFERENCES

[1] X. Shi, *Evaluation of Portland Cement Concrete Containing Reclaimed Asphalt Pavement for Pavement Applications*. PhD thesis, Texas A&M University, 2018.

[2] K. Rajagopal, "Conspectus of concepts of elasticity," *Mathematics and Mechanics of Solids*, vol. 16, no. 5, pp. 536–562, 2011.

[3] K. Rajagopal and J. Walton, "Modeling fracture in the context of a strain-limiting theory of elasticity: a single anti-plane shear crack," *International journal of fracture*, vol. 169, no. 1, pp. 39–48, 2011.

[4] Z. P. Bazant, *Fracture Mechanics of Concrete Structures: Proceedings of the First International Conference on Fracture Mechanics of Concrete Structures (FraMCoS1), held at Beaver Run Resort, Breckenridge, Colorado, USA, 1-5 June 1992.*, vol. 1. CRC Press, 1992.

[5] Z. Grasley, R. El-Helou, M. D'Ambrosia, D. Mokarem, C. Moen, and K. Rajagopal, "Model of infinitesimal nonlinear elastic response of concrete subjected to uniaxial compression," *Journal of Engineering Mechanics*, vol. 141, no. 7, 2015.

[6] S. Murakami, "Progress of continuum damage mechanics," *JSME international journal*, vol. 30, no. 263, pp. 701–710, 1987.

[7] J. Mazars, D. Boerman, and G. Piatti, "Mechanical damage and fracture of concrete structures," in *ICF5, Cannes (France) 1981*, 1981.

[8] B. Karihaloo and D. Fu, "An anisotropic damage model for plain concrete," *Engineering Fracture Mechanics*, vol. 35, no. 1-3, pp. 205–209, 1990.

[9] G. Pijaudier-Cabot and J. Mazars, "Damage models for concrete," *Handbook of materials behavior models*, vol. 2, pp. 500–512, 2001.

[10] Y. Calayir and M. Karaton, "A continuum damage concrete model for earthquake analysis of concrete gravity dam–reservoir systems," *Soil Dynamics and Earthquake Engineering*, vol. 25, no. 11, pp. 857–869, 2005.

[11] N. Masad, D. Zollinger, S.-M. Kim, and Z. Grasley, "Meso-scale model for simulations of concrete subjected to cryogenic temperatures," *Materials and Structures*, vol. 49, no. 6, pp. 2141–2159, 2016.

[12] P. Alagappan, K. Kannan, and K. Rajagopal, "On a possible methodology for identifying the initiation of damage of a class of polymeric materials," *Proceedings of the Royal Society A: Mathematical, Physical and Engineering Sciences*, vol. 472, no. 2192, p. 20160231, 2016.

[13] P. Alagappan, K. Rajagopal, and K. Kannan, "Initiation of damage in a class of polymeric materials embedded with multiple localized regions of lower density," *Mathematics and Mechanics of Solids*, p. 1081286517692392, 2017.

[14] D. Roylance, "Introduction to fracture mechanics," *Massachusetts Institute of Technology, Cambridge*, pp. 1–2, 2001.

[15] A. A. Griffith, "The phenomena of rupture and flow in solids," *Philosophical transactions of the royal society of london. Series A, containing papers of a mathematical or physical character*, vol. 221, pp. 163–198, 1921.

[16] Z. P. Bazant and J. Planas, *Fracture and size effect in concrete and other quasibrittle materials*, vol. 16. CRC press, 1997.

[17] G. R. Irwin, "Analysis of stresses and strains near the end of a crack traversing a plate," *Journal of applied mechanics*, vol. 24, no. 3, pp. 361–364, 1957.

[18] J. Mindess, "Young, and d. darwin, concrete," 2003.

[19] R. Swamy, *Linear elastic fracture mechanics parameters of concrete*. Elsevier Science Publishers, The Netherlands, 1983.

[20] S. Kumar and S. V. Barai, *Concrete fracture models and applications*. Springer Science & Business Media, 2011.

[21] H. Westergaard, "Bearing pressures and cra; c];< si," *Journal of applied mechanics*, vol. 18, 1939.

[22] M. Ohtsu, "Crack propagation in concrete: linear elastic fracture mechanics and boundary element method," *Theoretical and applied fracture mechanics*, vol. 9, no. 1, pp. 55–60, 1988.

[23] M. Wecharatana and S. Shah, *Nonlinear Fracture Mechanics Parameters*. Fracture Mechanics of Concrete, Amsterdam, The Netherlands: Elsevier Science Publishers B.V., 1983.

[24] V. O. Garcia-Alvarez, R. Gettu, and I. Carol, "Analysis of mixed-mode fracture in concrete using interface elements and a cohesive crack model," *Sadhana*, pp. 1–19, 2012.

[25] G. Irwin, J. Kies, and H. Smith, "Fracture strengths relative to onset and arrest of crack propagation," in *Proc. ASTM*, vol. 58, pp. 640–657, 1958.

[26] S. Kumar and S. Barai, "Cohesive crack model for the study of nonlinear fracture behaviour of concrete," *J Inst Eng (India), CV*, vol. 89, pp. 7–15, 2008.

[27] A. Hillerborg, M. Modéer, and P.-E. Petersson, "Analysis of crack formation and crack growth in concrete by means of fracture mechanics and finite elements," *Cement and concrete research*, vol. 6, no. 6, pp. 773–781, 1976.

[28] V. Gopalaratnam and B. Ye, "Numerical characterization of the nonlinear fracture process in concrete," *Engineering fracture mechanics*, vol. 40, no. 6, pp. 991–1006, 1991.

[29] A. S. Morgan, J. Niwa, and T. Tanabe, "Detecting the size effect in concrete beams using nonlinear fracture mechanics," *Engineering structures*, vol. 19, no. 8, pp. 605–616, 1997.

[30] S. S. Bhattacharjee and P. Léger, "Application of nlfm models to predict cracking in concrete gravity dams," *Journal of Structural Engineering*, vol. 120, no. 4, pp. 1255–1271, 1994.

[31] Z. P. Bažant and F.-B. Lin, "Nonlocal smeared cracking model for concrete fracture," *Journal of Structural Engineering*, vol. 114, no. 11, pp. 2493–2510, 1988.

[32] Y. Jenq and S. P. Shah, "Two parameter fracture model for concrete," *Journal of engineering mechanics*, vol. 111, no. 10, pp. 1227–1241, 1985.

[33] J. Mazars, "A description of micro-and macroscale damage of concrete structures," *Engineering Fracture Mechanics*, vol. 25, no. 5, pp. 729–737, 1986.

[34] J. Mazars, *Application de la mécanique de l'endommagement au comportement non linéaire et à la rupture du béton de structure*. PhD thesis, 1984.

[35] W. Brekelmans, P. Schreurs, and J. De Vree, "Continuum damage mechanics for softening of brittle materials," *Acta mechanica*, vol. 93, no. 1-4, pp. 133–143, 1992.

[36] H. Gang and H.-G. Kwak, "A strain rate dependent orthotropic concrete material model," *International Journal of Impact Engineering*, vol. 103, pp. 211–224, 2017.

[37] W. Zhu, J. Teng, and C. Tang, "Numerical simulation of strength envelope and fracture patterns of concrete under biaxial loading," *Magazine of Concrete Research*, vol. 54, no. 6, pp. 395–409, 2002.

[38] E. Chen, "Continuum damage response of a center-cracked plain concrete panel in tension," *Engineering fracture mechanics*, vol. 39, no. 3, pp. 553–560, 1991.

[39] F. Barzegar and S. Maddipudi, "Three-dimensional modeling of concrete structures. i: Plain concrete," *Journal of Structural Engineering*, vol. 123, no. 10, pp. 1339–1346, 1997.

[40] J. Lubliner, J. Oliver, S. Oller, and E. Onate, "A plastic-damage model for concrete," *International Journal of solids and structures*, vol. 25, no. 3, pp. 299–326, 1989.

[41] L. E. Malvern, *Introduction to the Mechanics of a Continuous Medium*. Prentice Hall, 1969.

[42] Cauchy and A. L. Baron, *Recherches sur l'équilibre et le mouvement intérieur des corps solides ou fluides, élastiques ou non élastiques*. 1822.

[43] C. Truesdell and W. Noll, "The non-linear field theories of mechanics," in *The non-linear field theories of mechanics*, pp. 1–579, Springer, 2004.

[44] Cauchy and AL, "Sur les equations qui exprement les conditions d'équilibre or les lois de mouvement interieur d'un corps solide," *Ex de Math*, vol. 3, pp. 160–187, 1828.

[45] M. Tasdemir, C. Tasdemir, S. Akyüz, A. Jefferson, F. Lydon, and B. Barr, "Evaluation of strains at peak stresses in concrete: a three-phase composite model approach," *Cement and Concrete Composites*, vol. 20, no. 4, pp. 301–318, 1998.

[46] R. Zouaoui, K. Miled, O. Limam, and A. Beddey, "Analytical prediction of aggregates' effects on the itz volume fraction and young's modulus of concrete," *International Journal for Numerical and Analytical Methods in Geomechanics*, vol. 41, no. 7, pp. 976–993, 2017.

[47] J. F. Young, S. Mindess, and D. Darwin, *Concrete*. Prentice Hall, 2002.

[48] S. Diamond and J. Huang, "The itz in concrete–a different view based on image analysis and sem observations," *Cement and concrete composites*, vol. 23, no. 2, pp. 179–188, 2001.

[49] K. L. Scrivener, A. K. Crumbie, and P. Laugesen, "The interfacial transition zone (itz) between cement paste and aggregate in concrete," *Interface Science*, vol. 12, no. 4, pp. 411–421, 2004.

[50] Y. Gao, G. De Schutter, G. Ye, Z. Tan, and K. Wu, "The itz microstructure, thickness and porosity in blended cementitious composite: Effects of curing age, water to binder ratio and aggregate content," *Composites part b: engineering*, vol. 60, pp. 1–13, 2014.

[51] W. Vichit-Vadakan and G. W. Scherer, "Measuring permeability of rigid materials by a beam-bending method: III, Cement Paste," *Journal of the American Ceramic Society*, vol. 85, no. 6, pp. 1537–1544, 2002.

[52] Z. Hashin and P. Monteiro, "An inverse method to determine the elastic properties of the interphase between the aggregate and the cement paste," *Cement and Concrete Research*, vol. 32, no. 8, pp. 1291–1300, 2002.

[53] W. Mathematica, "Wolfram research," *Inc., Champaign, Illinois*, 2009.

[54] Langer, Reid, and Dogan, *OOF: Finite Element Analysis of Microstructures*, 2017. `https://www.ctcms.nist.gov/oof/oof2/`.

[55] S. A. Langer, A. C. Reid, S. Haan, R. Garcia, R. Lua, and V. Coffman, "The oof2 manual," *NIST, US*, 2008.

[56] A. U. Manual, "Version 6.13-2," *Dassault Systémes Simulia Corp., Providence, Rhode Island, USA*, 2013.

[57] K. Rajagopal, "The elasticity of elasticity," *Zeitschrift für angewandte Mathematik und Physik*, vol. 58, no. 2, pp. 309–317, 2007.

[58] M. MatLab, "The language of technical computing," *The MathWorks, Inc. http://www. mathworks. com*, 2012.

[59] Z. Qian, E. Garboczi, G. Ye, and E. Schlangen, "Anm: a geometrical model for the composite structure of mortar and concrete using real-shape particles," *Materials and Structures*, vol. 49, no. 1-2, pp. 149–158, 2016.

[60] S. Thomas, Y. Lu, and E. Garboczi, "Improved model for three-dimensional virtual concrete: anm model," *Journal of Computing in Civil Engineering*, vol. 30, no. 2, p. 04015027, 2015.

[61] E. J. Garboczi, "Three-dimensional mathematical analysis of particle shape using x-ray tomography and spherical harmonics: Application to aggregates used in concrete," *Cement and concrete research*, vol. 32, no. 10, pp. 1621–1638, 2002.

[62] C. Yang, "Effect of the transition zone on the elastic moduli of mortar," *Cement and Concrete Research*, vol. 28, no. 5, pp. 727–736, 1998.

[63] Q. Li, F. Zhang, W. Zhang, and L. Yang, "Fracture and tension properties of roller compacted concrete cores in uniaxial tension," *Journal of Materials in Civil Engineering*, vol. 14, no. 5, pp. 366–373, 2002.

[64] L. M. Melis, A. H. Meyer, and D. W. Fowler, "An evaluation of tensile strength testing." Center for Transportation Research, University of Texas at Austin, 1985.

[65] X. Chen, S. Wu, and J. Zhou, "Variability of compressive strength of concrete cores," *Journal of Performance of Constructed Facilities*, vol. 28, no. 4, 2013.

[66] H.-S. Shang, T.-H. Yi, and Y.-P. Song, "Behavior of plain concrete of a high water-cement ratio after freeze-thaw cycles," *Materials*, vol. 5, no. 9, pp. 1698–1707, 2012.

[67] M. Königsberger, M. Hlobil, B. Delsaute, S. Staquet, C. Hellmich, and B. Pichler, "Hydrate failure in itz governs concrete strength: A micro-to-macro validated engineering mechanics model," *Cement and Concrete Research*, vol. 103, pp. 77–94, 2018.

[68] Y. Huang, Z. Yang, X. Chen, and G. Liu, "Monte Carlo simulations of meso-scale dynamic compressive behavior of concrete based on x-ray computed tomography images," *International Journal of Impact Engineering*, vol. 97, pp. 102–115, 2016.

[69] Y. Huang, D. Yan, Z. Yang, and G. Liu, "2d and 3d homogenization and fracture analysis of concrete based on in-situ x-ray computed tomography images and Monte Carlo simulations," *Engineering Fracture Mechanics*, vol. 163, pp. 37–54, 2016.

[70] K. Hassan, J. Brooks, and M. Erdman, "The use of reclaimed asphalt pavement (rap) aggregates in concrete," in *Waste management series*, vol. 1, pp. 121–128, Elsevier, 2000.

[71] A. Mukhopadhyay and X. Shi, "Microstructural characterization of portland cement concrete containing reclaimed asphalt pavement aggregates using conventional and advanced petrographic techniques," in *Advances in Cement Analysis and Concrete Petrography*, ASTM International, 2019.

[72] B. Huang, G. Li, D. Vukosavljevic, X. Shu, and B. K. Egan, "Laboratory investigation of mixing hot-mix asphalt with reclaimed asphalt pavement," *Transportation Research Record*, vol. 1929, no. 1, pp. 37–45, 2005.

[73] R. A. Tarefder, A. M. Zaman, and W. Uddin, "Determining hardness and elastic modulus of asphalt by nanoindentation," *International Journal of Geomechanics*, vol. 10, no. 3, pp. 106–116, 2010.

[74] B. Gérard, *Contribution of the mechanical, chemical and transport couplings in the long term behavior of radioactive waste repository structures*. PhD thesis, Ph. D. thesis, Laval University, Québec, Canada–Ecole Normale Supérieure de ..., 1996.

[75] D. Kuhl, F. Bangert, and G. Meschke, "An extension of damage theory to coupled chemo-mechanical processes," in *European Congress on Computational Methods in Applied Sciences and Engineering (ECCOMAS 2000), Barcelona, Spain. CD-Rom*, 2000.

[76] C. Le Bellégo, G. Pijaudier-Cabot, B. Gérard, J.-F. Dubé, and L. Molez, "Coupled mechanical and chemical damage in calcium leached cementitious structures," *Journal of Engineering Mechanics*, vol. 129, no. 3, pp. 333–341, 2003.

[77] C. Carde and R. François, "Aging damage model of concrete behavior during the leaching process," *Materials and Structures*, vol. 30, no. 8, pp. 465–472, 1997.

[78] F.-J. Ulm, J.-M. Torrenti, and F. Adenot, "Chemoporoplasticity of calcium leaching in concrete," *Journal of Engineering Mechanics*, vol. 125, no. 10, pp. 1200–1211, 1999.

[79] O. Coussy, *Mechanics of porous continua*. Wiley, 1995.

[80] F. Bangert, S. Grasberger, D. Kuhl, and G. Meschke, "Environmentally induced deterioration of concrete: physical motivation and numerical modeling," *Engineering Fracture Mechanics*, vol. 70, no. 7-8, pp. 891–910, 2003.

[81] M. Jebli, F. Jamin, C. Pelissou, E. Malachanne, E. Garcia-Diaz, and M. S. El Youssoufi, "Leaching effect on mechanical properties of cement-aggregate interface," *Cement and Concrete Composites*, vol. 87, pp. 10–19, 2018.

[82] C. Carde and R. François, "Effect of the leaching of calcium hydroxide from cement paste on mechanical and physical properties," *Cement and Concrete Research*, vol. 27, no. 4, pp. 539–550, 1997.

[83] Z. C. Grasley and K. R. Rajagopal, "Revisiting total, matric, and osmotic suction in partially saturated geomaterials," *Zeitschrift für angewandte Mathematik und Physik*, vol. 63, no. 2, pp. 373–394, 2012.

[84] S. C. Prasad and K. R. Rajagopal, "On the diffusion of fluids through solids undergoing large deformations," *Mathematics and mechanics of solids*, vol. 11, no. 3, pp. 291–305, 2006.

[85] L. Tao, J. Humphrey, and K. Rajagopal, "A mixture theory for heat-induced alterations in hydration and mechanical properties in soft tissues," *International Journal of Engineering Science*, vol. 39, no. 14, pp. 1535–1556, 2001.

[86] B. Huang and C. Qian, "Experiment study of chemo-mechanical coupling behavior of leached concrete," *Construction and Building Materials*, vol. 25, no. 5, pp. 2649–2654, 2011.

APPENDIX A

FIRST APPENDIX

The following is the VUMAT subroutine used to run the simulation on ABAQUS for the uni-axial tension and uni-axial compression cases using the generalized neo-Hookean model.

```
      subroutine vumat(nblock, ndi, nshr, nstatev, nfieldv, nprops,
     1     lanneal, stepTime, totTime, dt, cmname, coordMp,
     2     charLen, props, density, Dstrain, rSpinInc, temp0,
     3     U0, F0, field0, stressVec0, state0,
     4     intEne0, inelaEn0, temp1, U1,
     5     F1, field1, stressVec1, state1, intEne1, inelaEn1)
      include 'vaba_param.inc'
      integer nblock, ndi, nshr, nstatev, nfieldv, nprops, lanneal
      real stepTime, totTime, dt, r, ri,r0,rmid
      character*80 cmname
      real coordMp(nblock,*)
      integer charLen
      real props(nprops), density(nblock),
     1     Dstrain(nblock,ndi+nshr), rSpinInc(nblock,nshr),
     2     temp0(nblock), U0(nblock,ndi+nshr),
     3     F0(nblock,ndi+nshr+nshr), field0(nblock,nfieldv),
     4     stressVec0(nblock,ndi+nshr), state0(nblock,nstatev),
     5     intEne0(nblock), inelaEn0(nblock), temp1(nblock),
     6     U1(nblock,ndi+nshr), F1(nblock,ndi+nshr+nshr),
     7     field1(nblock,nfieldv), stressVec1(nblock,ndi+nshr),
     8     state1(nblock,nstatev), intEne1(nblock), inelaEn1(nblock)
```

```
c     local variables
      real F(3,3), E(3,3), J, t1, t2, t3, mu, kappa, trT
      integer i
         trT= stressVec0(i,1)+stressVec0(i,2)+stressVec0(i,3)
         if (cmname .eq. "ITZ") then
          mu=5000
          kappa=mu*1.3
          else if (cmname .eq. "AGGREGATE") then
          mu=23000
          kappa=mu*1.3
          else if (cmname .eq. "CEMENT") then
          mu=15000
          kappa=mu*1.3
          end if
c     loop through all blocks
      do i = 1, nblock
c        setup F (upper diagonal part)
         F(1,1) = U1(i,1)
         F(2,2) = U1(i,2)
         F(3,3) = U1(i,3)
         F(1,2) = U1(i,4)
         if (nshr .eq. 1) then
            F(2,3) = 0.0
            F(1,3) = 0.0
         else
            F(2,3) = U1(i,5)
            F(1,3) = U1(i,6)
```

```
      end if
      t1 = F(1,1) * (F(2,2)*F(3,3) - F(2,3)**2)
      t2 = F(1,2) * (F(2,3)*F(1,3) - F(1,2)*F(3,3))
      t3 = F(1,3) * (F(1,2)*F(2,3) - F(2,2)*F(1,3))
      J = t1 + t2 + t3
      t1 = J**(-2.0/3.0)
C
      E(1,1) = t1*(F(1,1)+F(1,1)-1)
      E(2,2) = t1*(F(2,2)+F(2,2)-1)
      E(3,3) = t1*(F(3,3)+F(3,3)-1)
      E(1,2) = t1*(F(1,2)+F(2,1))
      E(1,3) = t1*(F(1,3)+F(3,1))
      E(2,3) = t1*(F(2,3)+F(3,2))
C
      t1 = (E(1,1) + E(2,2) + E(3,3)) / 3.0
      t2 = mu/(J**15)  !/25
      t3 = kappa*(J-1)/(J**15)
      if (J > 1.00002) then
         state1(i,1)=0
      else
         state1(i,1)=1
      end if
      state1(i,1)=(1/J)*100
      StressVec1(i,1) = t2*alpha * (E(1,1) - t1) + t3*beta
      StressVec1(i,2) = t2*alpha * (E(2,2) - t1) + t3*beta
      StressVec1(i,3) = t2*alpha * (E(3,3) - t1) + t3*beta
      StressVec1(i,4) = t2*alpha * E(1,2)
```

```
            if (nshr .eq. 3) then
               StressVec1(i,5) = t2*alpha * E(2,3)
               StressVec1(i,6) = t2*alpha * E(1,3)
            end if
         end do
         return
         end
```

The UMAT subroutine given below is used to run the preliminary simulation on ABAQUS for the uni-axial tension case using the linearized strain based implicit constitutive theory, in order to decide the threshold density value for element deletion.

```
      SUBROUTINE UMAT(STRESS,STATEV,DDSDDE,SSE,SPD,SCD,
     1 RPL,DDSDDT,DRPLDE,DRPLDT,
     2 STRAN,DSTRAN,TIME,DTIME,TEMP,DTEMP,PREDEF,DPRED,CMNAME,
     3 NDI,NSHR,NTENS,NSTATV,PROPS,NPROPS,COORDS,DROT,PNEWDT,
     4 CELENT,DFGRD0,DFGRD1,NOEL,NPT,LAYER,KSTEP,KSPT,KINC)
C
      INCLUDE 'ABA_PARAM.INC'
C
      CHARACTER*80 CMNAME
      DIMENSION STRESS(NTENS),STATEV(NSTATV),
     1 DDSDDE(NTENS,NTENS),DDSDDT(NTENS),DRPLDE(NTENS),
     2 STRAN(NTENS),DSTRAN(NTENS),TIME(2),PREDEF(1),DPRED(1),
     3 PROPS(NPROPS),COORDS(3),DROT(3,3),DFGRD0(3,3),DFGRD1(3,3)
C     ELASTIC USER SUBROUTINE
      PARAMETER(ONE=1.D0,TWO=2.D0,POINTTHREE=0.3D0)
      EMOD=PROPS(1)
      ANU=PROPS(2)
```

```
      RHO=PROPS(3)
      ALPHA=POINTTHREE
C
      DDSDDE(2,2)=(EMOD/(ONE-(ANU*ANU)))*(ONE-(ALPHA*RHO*
      ((ONE-(TW0*ANU))/(ONE-ANU))*((TWO*STRAN(2))+((ANU+ONE)*
      STRAN(1)))))
      DDSDDE(1,1)=(EMOD/(ONE-(ANU*ANU)))*(ONE-(ALPHA*RHO*
      ((ONE-(TW0*ANU))/(ONE-ANU))*((TWO*STRAN(1))+((ANU+ONE)*
      STRAN(2)))))
      DDSDDE(1,2)=(EMOD/(ONE-(ANU*ANU)))*(ANU-(ALPHA*RHO*
      ((ONE-(TW0*ANU))/(ONE-ANU))*((TWO*ANU*STRAN(2))+((ANU+ONE)*
      STRAN(1)))))
      DDSDDE(2,1)=(EMOD/(ONE-(ANU*ANU)))*(ANU-(ALPHA*RHO*
      ((ONE-(TW0*ANU))/(ONE-ANU))*((TWO*ANU*STRAN(1))+((ANU+ONE)*
      STRAN(2)))))
      DDSDDE(3,3)=(EMOD/(ONE+ANU))*(ONE-(ALPHA*RHO*
      (((TWO*ANU)-ONE)/(ANU-ONE))*(STRAN(1)+STRAN(2))))
      STATEV(1)=(((TWO*ANU)-ONE)/(ANU-ONE))*(STRAN(1)+STRAN(2))
      STATEV(2)=EMOD*(ONE-(ALPHA*RHO*STATEV(1)))
      DO K2=1,NTENS
       DO K3=1,NTENS
         STRESS(K2)=STRESS(K2)+(DDSDDE(K2,K3)*DSTRAN(K3))
       ENDDO
      ENDDO
      RETURN
      END
```

The following VUMAT subroutine is used to run the simulations of uni-axial tension and uni-

axial compression using the linearized strain based implicit constitutive theory on ABAQUS.

```
      subroutine vumat(nblock, ndi, nshr, nstatev, nfieldv, nprops,
     1     lanneal, stepTime, totTime, dt, cmname, coordMp,
     2     charLen, props, density, Dstrain, rSpinInc, temp0,
     3     U0, F0, field0, stressVec0, state0,
     4     intEne0, inelaEn0, temp1, U1,
     5     F1, field1, stressVec1, state1, intEne1, inelaEn1)
      include 'vaba_param.inc'
      integer nblock, ndi, nshr, nstatev, nfieldv, nprops, lanneal
      real stepTime, totTime, dt, r, ri,r0,rmid
      character*80 cmname
      real coordMp(nblock,*)
      integer charLen
      real props(nprops), density(nblock),
     1     Dstrain(nblock,ndi+nshr), rSpinInc(nblock,nshr),
     2     temp0(nblock), U0(nblock,ndi+nshr),
     3     F0(nblock,ndi+nshr+nshr), field0(nblock,nfieldv),
     4     stressVec0(nblock,ndi+nshr), state0(nblock,nstatev),
     5     intEne0(nblock), inelaEn0(nblock), temp1(nblock),
     6     U1(nblock,ndi+nshr), F1(nblock,ndi+nshr+nshr),
     7     field1(nblock,nfieldv), stressVec1(nblock,ndi+nshr),
     8     state1(nblock,nstatev), intEne1(nblock), inelaEn1(nblock)
c     local variables
      real F(3,3), E(3,3), J, t1, t2, t3, mu, kappa, trT, trE
      integer i
         trT= stressVec0(i,1)+stressVec0(i,2)+stressVec0(i,3)
         if (cmname .eq. "ITZ") then
```

```
            rho=1100
            nu=0.2
            emod=12000
            else if (cmname .eq. "AGGREGATE") then
            rho=2700
            nu=0.2
            emod=55200
            else
            rho=2200
            nu=0.2
            emod=36000
            end if
c     loop through all blocks
      do i = 1, nblock
c        setup F (upper diagonal part)
         F(1,1) = U1(i,1)
         F(2,2) = U1(i,2)
         F(3,3) = U1(i,3)
         F(1,2) = U1(i,4)
         if (nshr .eq. 1) then
            F(2,3) = 0.0
            F(1,3) = 0.0
         else
            F(2,3) = U1(i,5)
            F(1,3) = U1(i,6)
         end if
         E(1,1) = F(1,1)-1
```

```
      E(2,2) = F(2,2)-1
      E(3,3) = F(3,3)-1
      E(1,2) = F(1,2)
      E(1,3) = F(1,3)
      E(2,3) = F(2,3)
      trE = (E(1,1) + E(2,2) + E(3,3))
      t2 = nu
      t3 = emod*(1-(alpha*rho*trE))
      state1(i,1)=trE
      state1(i,2)=emod*(1-(alpha*rho*trE))
      if (state1(i,1) > 0.00075) then
         state1(i,3)=0
      else
         state1(i,3)=1
      end if
      StressVec1(i,1) = ((t3/(1+t2))*E(1,1)) + ((t2/(1+t2))*trT)
      StressVec1(i,2) = ((t3/(1+t2))*E(2,2)) + ((t2/(1+t2))*trT)
      StressVec1(i,3) = ((t3/(1+t2))*E(3,3)) + ((t2/(1+t2))*trT)
      StressVec1(i,4) = ((t3/(1+t2))*E(1,2))
      if (nshr .eq. 3) then
         StressVec1(i,5) = (2*t2*E(2,3))
         StressVec1(i,6) = (2*t2*E(1,3))
      end if
   end do
   return
   end
```

The following subroutine code is for the case where concrete exposed to leaching for 28 days

is subjected to uni-axial compression and the sub-case based on the assumption that CH is leached from both paste and the ITZ.

```
      subroutine vumat(nblock, ndi, nshr, nstatev, nfieldv, nprops,
     1     lanneal, stepTime, totTime, dt, cmname, coordMp,
     2     charLen, props, density, Dstrain, rSpinInc, temp0,
     3     U0, F0, field0, stressVec0, state0,
     4     intEne0, inelaEn0, temp1, U1,
     5     F1, field1, stressVec1, state1, intEne1, inelaEn1)
      include 'vaba_param.inc'
      integer nblock, ndi, nshr, nstatev, nfieldv, nprops, lanneal
      real stepTime, totTime, dt, r, ri,r0,rmid
      character*80 cmname
      real coordMp(nblock,*)
      integer charLen
      real props(nprops), density(nblock),
     1     Dstrain(nblock,ndi+nshr), rSpinInc(nblock,nshr),
     2     temp0(nblock), U0(nblock,ndi+nshr),
     3     F0(nblock,ndi+nshr+nshr), field0(nblock,nfieldv),
     4     stressVec0(nblock,ndi+nshr), state0(nblock,nstatev),
     5     intEne0(nblock), inelaEn0(nblock), temp1(nblock),
     6     U1(nblock,ndi+nshr), F1(nblock,ndi+nshr+nshr),
     7     field1(nblock,nfieldv), stressVec1(nblock,ndi+nshr),
     8     state1(nblock,nstatev), intEne1(nblock), inelaEn1(nblock)
c     local variables
      real F(3,3), E(3,3), J, t1, t2, t3, mu, kappa, trT, trE
      integer i
         trT= stressVec0(i,1)+stressVec0(i,2)+stressVec0(i,3)
```

```
            if (cmname .eq. "ITZ") then
             rho=1026.67
             nu=0.2
             emod=9756.444444
             else if (cmname .eq. "AGGREGATE") then
             emod=55200
             rho=2700
             nu=0.25
             else
             rho=2053.333333
             nu=0.2
             emod=29269.33
             end if
c      loop through all blocks
       do i = 1, nblock
c         setup F (upper diagonal part)
          F(1,1) = U1(i,1)
          F(2,2) = U1(i,2)
          F(3,3) = U1(i,3)
          F(1,2) = U1(i,4)
          if (nshr .eq. 1) then
             F(2,3) = 0.0
             F(1,3) = 0.0
          else
             F(2,3) = U1(i,5)
             F(1,3) = U1(i,6)
          end if
```

```
          alpha=0.01
c
          E(1,1) = F(1,1)-1
          E(2,2) = F(2,2)-1
          E(3,3) = F(3,3)-1
          E(1,2) = F(1,2)
          E(1,3) = F(1,3)
          E(2,3) = F(2,3)
          trE = (E(1,1) + E(2,2) + E(3,3))
          t2 = nu
          t3 = emod*(1-(alpha*rho*trE))
          state1(i,1)=trE
          state1(i,2)=rho*(1-(alpha*rho*trE))
          StressVec1(i,1) = ((t3/(1+t2))*E(1,1)) + ((t2/(1+t2))*trT)
          StressVec1(i,2) = ((t3/(1+t2))*E(2,2)) + ((t2/(1+t2))*trT)
          StressVec1(i,3) = ((t3/(1+t2))*E(3,3)) + ((t2/(1+t2))*trT)
          StressVec1(i,4) = ((t3/(1+t2))*E(1,2))
          if (nshr .eq. 3) then
             StressVec1(i,5) = (2*t2*E(2,3))
             StressVec1(i,6) = (2*t2*E(1,3))
          end if
       end do
       return
       end
```

The following VUMAT subroutine for the case where concrete is exposed to leaching to CH while being subjected to uni-axial compression simultaneously. It is for the sub-case based on the assumption that both paste and the ITZ are being leached out of CH.

```
      subroutine vumat(nblock, ndi, nshr, nstatev, nfieldv, nprops,
     1     lanneal, stepTime, totTime, dt, cmname, coordMp,
     2     charLen, props, density, Dstrain, rSpinInc, temp0,
     3     U0, F0, field0, stressVec0, state0,
     4     intEne0, inelaEn0, temp1, U1,
     5     F1, field1, stressVec1, state1, intEne1, inelaEn1)
      include 'vaba_param.inc'
      integer nblock, ndi, nshr, nstatev, nfieldv, nprops, lanneal
      real stepTime, totTime, dt, r, ri,r0,rmid
      character*80 cmname
      real coordMp(nblock,*)
      integer charLen
      real props(nprops), density(nblock),
     1     Dstrain(nblock,ndi+nshr), rSpinInc(nblock,nshr),
     2     temp0(nblock), U0(nblock,ndi+nshr),
     3     F0(nblock,ndi+nshr+nshr), field0(nblock,nfieldv),
     4     stressVec0(nblock,ndi+nshr), state0(nblock,nstatev),
     5     intEne0(nblock), inelaEn0(nblock), temp1(nblock),
     6     U1(nblock,ndi+nshr), F1(nblock,ndi+nshr+nshr),
     7     field1(nblock,nfieldv), stressVec1(nblock,ndi+nshr),
     8     state1(nblock,nstatev), intEne1(nblock), inelaEn1(nblock)
c     local variables
      real F(3,3), E(3,3), J, t1, t2, t3, trT, trE, slope, por
      integer i
         trT= stressVec0(i,1)+stressVec0(i,2)+stressVec0(i,3)
         if (cmname .eq. "ITZ") then
          rho=1100
```

```
            nu=0.2
            emod=12000
            slope=6.67
            else if (cmname .eq. "AGGREGATE") then
            rho=2700
            nu=0.25
            emod=55200
            slope=0
            else
            rho=2200
            nu=0.2
            emod=36000
            slope=6.67
            end if
c     loop through all blocks
      do i = 1, nblock
c        setup F (upper diagonal part)
         F(1,1) = U1(i,1)
         F(2,2) = U1(i,2)
         F(3,3) = U1(i,3)
         F(1,2) = U1(i,4)
         if (nshr .eq. 1) then
            F(2,3) = 0.0
            F(1,3) = 0.0
         else
            F(2,3) = U1(i,5)
            F(1,3) = U1(i,6)
```

```
      end if
      alpha=0.001
      por=slope*stepTime/100
      E(1,1) = F(1,1)-1
      E(2,2) = F(2,2)-1
      E(3,3) = F(3,3)-1
      E(1,2) = F(1,2)
      E(1,3) = F(1,3)
      E(2,3) = F(2,3)
      trE = (E(1,1) + E(2,2) + E(3,3))
      t2 = nu
      t3 = emod*(1-(alpha*(rho-(rho*(1-por)*(1-trE)))))
      state1(i,1)=trE
      state1(i,2)=rho*(1-por)*(1-state1(i,1))
      state1(i,3)=emod*(1-(alpha*(rho-state1(i,2))))
      StressVec1(i,1) = ((t3/(1+t2))*E(1,1)) + ((t2/(1+t2))*trT)
      StressVec1(i,2) = ((t3/(1+t2))*E(2,2)) + ((t2/(1+t2))*trT)
      StressVec1(i,3) = ((t3/(1+t2))*E(3,3)) + ((t2/(1+t2))*trT)
      StressVec1(i,4) = ((t3/(1+t2))*E(1,2))
      if (nshr .eq. 3) then
         StressVec1(i,5) = (2*t2*E(2,3))
         StressVec1(i,6) = (2*t2*E(1,3))
      end if
   end do
   return
   end
```

The VUMAT subroutine give below is for the simulation of uni-axial compression of RAP-PCC

microstructure.

```
      subroutine vumat(nblock, ndi, nshr, nstatev, nfieldv,
      nprops,
     1     lanneal, stepTime, totTime, dt, cmname, coordMp,
     2     charLen, props, density, Dstrain, rSpinInc, temp0,
     3     U0, F0, field0, stressVec0, state0,
     4     intEne0, inelaEn0, temp1, U1,
     5     F1, field1, stressVec1, state1, intEne1, inelaEn1)
      include 'vaba_param.inc'
      integer nblock, ndi, nshr, nstatev, nfieldv, nprops, lanneal
      real stepTime, totTime, dt, r, ri,r0,rmid
      character*80 cmname
      real coordMp(nblock,*)
      integer charLen
      real props(nprops), density(nblock),
     1     Dstrain(nblock,ndi+nshr), rSpinInc(nblock,nshr),
     2     temp0(nblock), U0(nblock,ndi+nshr),
     3     F0(nblock,ndi+nshr+nshr), field0(nblock,nfieldv),
     4     stressVec0(nblock,ndi+nshr), state0(nblock,nstatev),
     5     intEne0(nblock), inelaEn0(nblock), temp1(nblock),
     6     U1(nblock,ndi+nshr), F1(nblock,ndi+nshr+nshr),
     7     field1(nblock,nfieldv), stressVec1(nblock,ndi+nshr),
     8     state1(nblock,nstatev), intEne1(nblock), inelaEn1(nblock)
c     local variables
      real F(3,3), E(3,3), J, t1, t2, t3, mu, kappa, trT, trE
      integer i
         trT= stressVec0(i,1)+stressVec0(i,2)+stressVec0(i,3)
```

```
            if (cmname .eq. "ITZ") then
             rho=1100
             nu=0.2
             emod=12000
             else if (cmname .eq. "AGGREGATE") then
             rho=2510
             nu=0.25
             emod=55200
             else if (cmname .eq. "PASTE") then
             rho=2200
             nu=0.2
             emod=34000
             else
             rho=1030
             nu=0.25
             emod=1500
             end if
c      loop through all blocks
       do i = 1, nblock
c         setup F (upper diagonal part)
          F(1,1) = U1(i,1)
          F(2,2) = U1(i,2)
          F(3,3) = U1(i,3)
          F(1,2) = U1(i,4)
          if (nshr .eq. 1) then
             F(2,3) = 0.0
             F(1,3) = 0.0
```

```
      else
         F(2,3) = U1(i,5)
         F(1,3) = U1(i,6)
      end if
     alpha=0.001
c
      E(1,1) = F(1,1)-1
      E(2,2) = F(2,2)-1
      E(3,3) = F(3,3)-1
      E(1,2) = F(1,2)
      E(1,3) = F(1,3)
      E(2,3) = F(2,3)
      trE = (E(1,1) + E(2,2) + E(3,3))
      t2 = nu
      t3 = emod*(1-(alpha*rho*trE))
      state1(i,1)=trE
      StressVec1(i,1) = ((t3/(1+t2))*E(1,1)) + ((t2/(1+t2))*trT)
      StressVec1(i,2) = ((t3/(1+t2))*E(2,2)) + ((t2/(1+t2))*trT)
      StressVec1(i,3) = ((t3/(1+t2))*E(3,3)) + ((t2/(1+t2))*trT)
      StressVec1(i,4) = ((t3/(1+t2))*E(1,2))
      if (nshr .eq. 3) then
         StressVec1(i,5) = (2*t2*E(2,3))
         StressVec1(i,6) = (2*t2*E(1,3))
      end if
    end do
    return
    end
```

APPENDIX B

SECOND APPENDIX

The meshes for different microstructures used for modeling in the current research are shown in Figures B.1, B.2, B.3, and B.4. The features of these are presented in Table B.1.

Table B.1: Features of the mesh for different microstructures

Microstructure	Nodes	Elements	Linear quadrilateral element type CPS4R	Linear triangular element type CPS3
Neo-Hookean microstructure	81262	121305	41048	80257
D3-M Microstructure 1	54893	80119	29611	50508
D3-M Microstructure 2	54304	79127	29178	49949
D3-M Microstructure 3	55484	80880	29765	51115

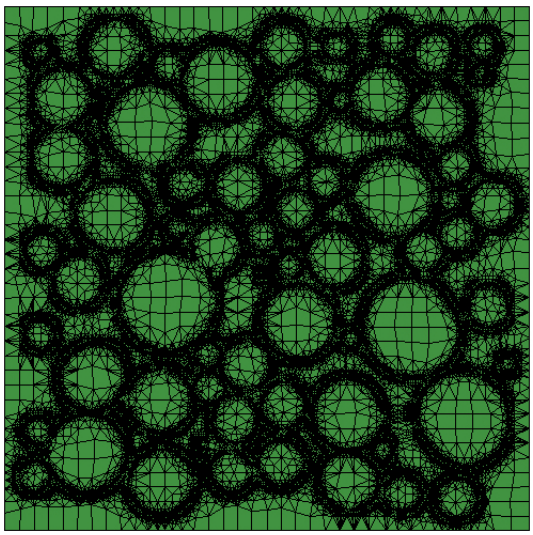

Figure B.1: Mesh for Microstructure used to model the response of concrete to uni-axial tension and uni-axial compression based on generalized neo-Hookean model

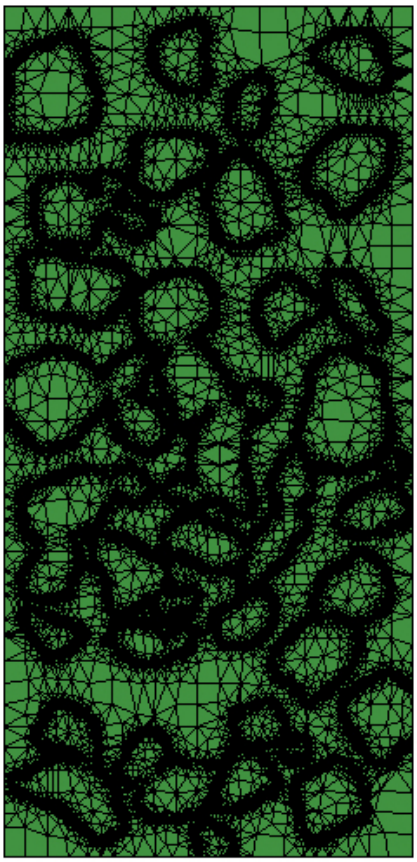

Figure B.2: Mesh for Microstructure 1 used to model the response of concrete to uni-axial tension and uni-axial compression based on density driven damage mechanics (D3-M) approach

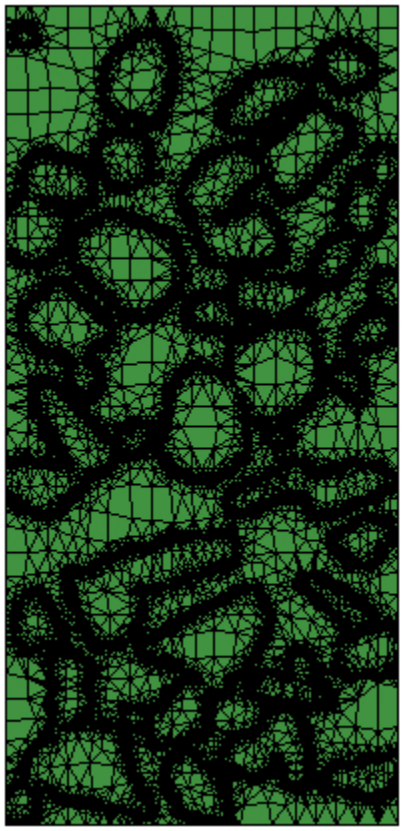

Figure B.3: Mesh for Microstructure 2 used to model the response of concrete to uni-axial tension and uni-axial compression based on density driven damage mechanics (D3-M) approach

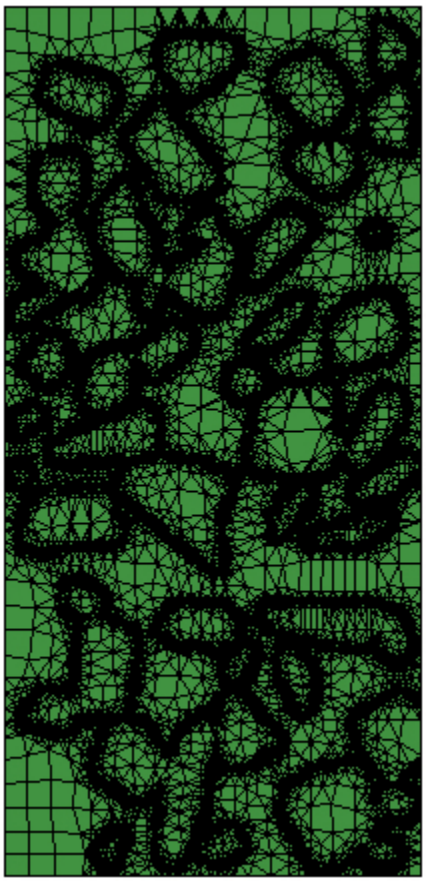

Figure B.4: Mesh for Microstructure 3 used to model the response of concrete to uni-axial tension and uni-axial compression based on density driven damage mechanics (D3-M) approach